Propofol-mediated Unconsciousness Disrupts Progression of Sensory Signals through the Cortical Hierarchy

John M. Tauber[1], Scott L. Brincat[1], Emily P. Stephen[2], Jacob A. Donoghue[1], Leo Kozachkov[1], Emery N. Brown[1,3,4*], and Earl K. Miller[1*]

Abstract

■ A critical component of anesthesia is the loss of sensory perception. Propofol is the most widely used drug for general anesthesia, but the neural mechanisms of how and when it disrupts sensory processing are not fully understood. We analyzed local field potential and spiking recorded from Utah arrays in auditory cortex, associative cortex, and cognitive cortex of nonhuman primates before and during propofol-mediated unconsciousness. Sensory stimuli elicited robust and decodable stimulus responses and triggered periods of stimulus-related synchronization between brain areas in the local field potential of Awake animals. By contrast, propofol-mediated unconsciousness eliminated stimulus-related synchrony and drastically weakened stimulus responses and information in all brain areas except for auditory cortex, where responses and information persisted. However, we found stimuli occurring during spiking Up states triggered weaker spiking responses than in Awake animals in auditory cortex, and little or no spiking responses in higher order areas. These results suggest that propofol's effect on sensory processing is not just because of asynchronous Down states. Rather, both Down states and Up states reflect disrupted dynamics. ■

INTRODUCTION

General anesthesia is used in nearly 60,000 procedures every day in the United States (Brown, Lydic, & Schiff, 2010). A critical component of general anesthesia is unconsciousness, during which a patient is unaware of their environment (Brown et al., 2010). Intraoperative awareness occurs when this goal is not achieved (Ghoneim, 2000). Although the phenomenon is rare (Sebel et al., 2004), patients that experience it report severe trauma (Kotsovolis & Komninos, 2009). Most studies of anesthetic effects on the brain have focused on physiological state change. However, if we are to understand how anesthesia renders unconsciousness and how this fails in intraoperative awareness, we need to understand its effects on processing of sensory inputs. We aimed to do so using propofol, one of the most commonly used anesthetics.

Propofol is a gamma-aminobutyric acid-agonist (Hemmings et al., 2005, 2019; Bai, Pennefather, MacDonald, & Orser, 1999). Although propofol's molecular mechanism of action is well understood (Sahinovic, Struys, & Absalom, 2018), we have less understanding of how it works at the level of functioning networks (Lewis et al., 2012, 2013; Purdon et al., 2013; Brown, Purdon, & Van Dort, 2011). Propofol induces overall increases in slow oscillations (0.1–4 Hz) in EEG and local field potential (LFP) recordings, and a broad reduction in spiking activity (Bastos et al., 2021; Redinbaugh et al., 2020; Purdon, Sampson, Pavone, & Brown, 2015). Spiking becomes strongly coupled to the phase of the slow oscillations, creating alternating irregular "Up" and "Down" states of high and low activity, respectively (Bastos et al., 2021; Lewis et al., 2012). This may disrupt long-range synchronization between cortical regions, a putative mechanism for cortical communication (Bastos et al., 2021; Redinbaugh et al., 2020; Pesaran et al., 2018; Fries, 2015; Crowe et al., 2013; Lewis et al., 2012). Support for this comes from observations that sensory responses are weakened in higher cortex but can be preserved in lower (sensory) cortex (Nourski et al., 2017, 2021; Krom et al., 2020; Ishizawa et al., 2016). However, few studies, especially in animals, have followed the chain of sensory processing from lower to higher cortex.

We did so using data collected in two nonhuman primates (NHPs) from our previous study on propofol anesthesia (Bastos et al., 2021). We compared and contrasted cortical responses to auditory and tactile stimulation before and after loss of consciousness (LOC). This analysis includes simultaneous recordings of LFP and spiking activity from multiple cortical levels: sensory (temporal) cortex, associative (parietal) cortex, and higher (frontal) cortex. Our results suggest propofol anesthesia leaves intact sensory processing in the sensory cortex, but these signals fail to be transmitted to higher level cortical areas.

[1]Massachusetts Institute of Technology, Cambridge, MA, [2]Boston University, MA, [3]Massachusetts General Hospital, Boston, [4]Harvard University, Cambridge, MA
*Co-senior PIs.

Journal of Cognitive Neuroscience 36:2, pp. 394–413
https://doi.org/10.1162/jocn_a_02081

METHODS

Experimental

Two NHPs (rhesus macaques: *Macaca mulatta*) participated in the study (Bastos et al., 2021). NHP 1 was male, aged 14 years and weighed 13.0 kg. NHP 2 was female, aged 7 years and weighed 5.0 kg. Twenty-one sessions (11 from NHP 1, 10 from NHP 2) were used. Each session consisted of 15–90 min of Awake baseline electrophysiological recordings. Then propofol was intravenously infused via a computer-controlled syringe pump. To induce unconsciousness, a high-rate infusion was given for 30 min (285 μg/kg/min for NHP 1; 580 μg/kg/min for NHP 2). Immediately following the high-rate infusion was 30 min of a maintenance dose (142.5 μg/kg/min for NHP 1; 320 μg/kg/min for NHP 2). The infusion rates were determined based on the animals' age and weight. Infusion was performed via a subcutaneous vascular access port at the cervicothoracic junction of the neck with the catheter tip reaching the termination of the superior vena cava via the external jugular vein. The animals were neither paralyzed nor intubated in the experiments. Both NHPs were chronically implanted with four 8 × 8 iridium-oxide contact microelectrode arrays (Utah arrays, MultiPort: 1.0-mm shank length, 400-μm spacing, Blackrock Microsystems), for 256 electrodes. Arrays were implanted in the prefrontal (Area 46 ventral and 8A), posterior parietal (Area 7A/7B), and temporal-auditory (caudal parabelt area STG [superior temporal gyrus]) cortices. We refer to the recorded brain areas in the text as STG, posterior parietal cortex (PPC), Region 8A (8A), and ventrolateral prefrontal cortex (vlPFC; Figure 1A).

LFPs were recorded at 30 kHz and filtered online via a lowpass 250-Hz software filter and downsampled to 1 kHz. Spiking activity was recorded by sampling the raw analog signal at 30 kHz, bandpass filtered from 250 Hz to 5 kHz, and manually thresholding. Blackrock Cereplex E headstages were utilized for digital recording via two to three synchronized Blackrock Cerebus Digital Acquisition systems. Single units were sorted manually offline using principal component analysis with commercially available software (Offline Sorter v4, Plexon Inc.). All other preprocessing and analyses were performed with MATLAB (The Mathworks, Inc.). The number of sorted units per brain area differed between NHP 1 and NHP 2, and also differed slightly across sessions. For NHP 1: ~50 units were recorded in STG, ~80 in PPC, ~40 in 8A, and ~40 in vlPFC. For NHP 2: one to five units were recorded in STG, ~20 in PPC, ~20 in 8A, and ~80 in vlPFC. For further information on neural recording and propofol delivery methods, see Bastos and colleagues (2021). All procedures followed the guidelines of the MIT Animal Care and Use Committee (Protocol Number 0619–035-22) and the U.S. National Institutes of Health.

Three different stimuli were presented to the NHPs throughout each session to characterize sensory processing under anesthesia (Figure 1B). Two distinct brief (500 msec) auditory tones were used. The first ("Cond Tone" [conditioned tone]) consisted of a pure (constant frequency) tone and always preceded an airpuff ("Cond Puff" [conditioned puff]; 16–18 psi, Airstim, *SD*-Instruments) by 500 msec. The second was a ringing tone and was presented alone ("UC Tone" [unconditioned tone]). An airpuff, identical to the Cond Puff, was also presented alone ("UC Puff" [unconditioned puff]). Facial movements were monitored throughout the experimental sessions (Eyelink 1000 Plus, SR-Research), and the LOC (Figure 1C) was determined by the moment the eyes closed and remained closed for the remainder of the infusion (i.e., not responding to airpuffs). Recovery of consciousness (ROC; Figure 1C) was marked when the eyes opened after cessation of propofol administration.

We analyzed the cortical responses to sensory stimuli under two different conditions: Awake (before administration of propofol) versus Unconscious (after LOC, during the maintenance dose). Data from the maintenance dose were used for two reasons. First, the brain state was unchanging during the maintenance dose (Figure 1C). This consistency allowed for more reliable data pooling across stimulus presentations and comparison with the pre-anesthesia Awake state, which was also consistent over time. Second, the maintenance dose was designed to mimic the portion of human clinical procedures when there is also steady-state maintenance. Thus, understanding how propofol alters cortical sensory processing has the most clinical relevance during this interval.

Sensory stimuli were delivered continuously throughout the experimental sessions. They were spaced approximately 5 sec apart, randomly interleaved, and provided samples sizes comparable to previous studies (Ishizawa et al., 2016; Purdon et al., 2013). In the Awake state, the average number of stimulus presentations in a given session was 67 (range: 47–80) for UC Tone, 67 (57–75) for UC Puff, and 67 (58–84) for Cond Tone/Cond Puff. In the Unconscious state, the average was 78 (range: 68–89) for UC Tone, 74 (61–100) for UC Puff, and 73 (61–84) for Cond Tone/Cond Puff.

We used data from both NHPs in our analyses of LFP data (Figures 3–5), where data quality and results were consistent across animals. We excluded areas STG, PPC, and 8A in NHP 2 from the analysis of spiking responses (Figure 6). In the STG of NHP 2, we were unable to resolve Up and Down states because of the low number of neurons. Up states were observed in the PPC and 8A of NHP 2, but had very short duration, and hence too few stimuli occurred within them to estimate a response with high confidence. Because our LFP results were consistent across animals and sessions, and the spiking results for NHP1 were in agreement with prior studies, inclusion of these results is in line with the *Journal of Cognitive Neuroscience*'s policy for NHP studies (Fries & Maris, 2022).

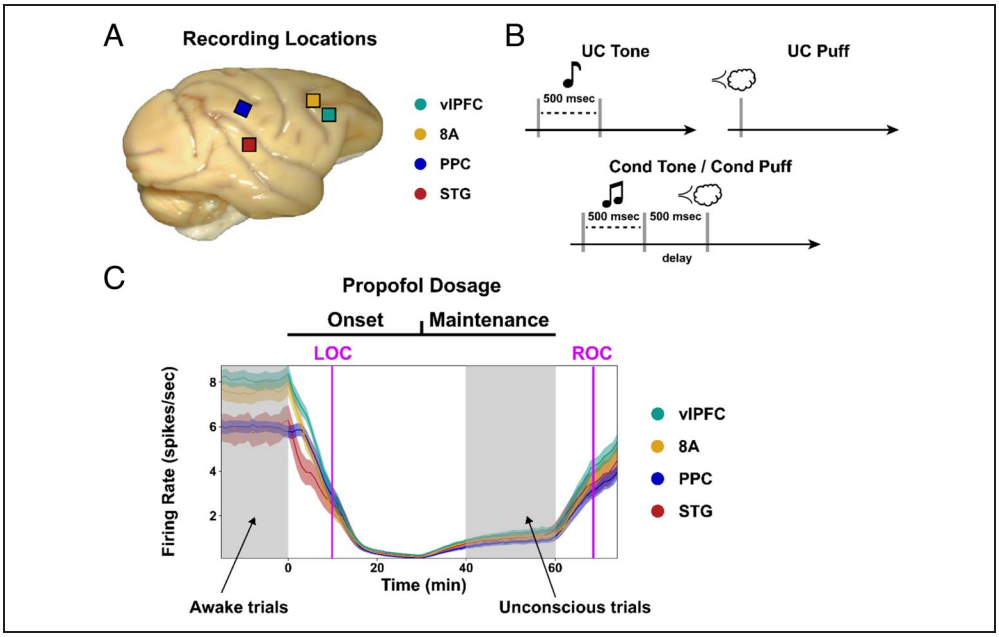

Figure 1. LFP and spiking data were recorded from four cortical areas whereas stimuli were delivered in Awake and Unconscious animals. (A) Implanted locations of Utah arrays. STG (auditory); PPC (associative); 8A (cognitive); vlPFC (cognitive). (B) Stimuli delivered during Awake and Unconscious states. UC (unconditioned) Tone and Cond Tone are two distinct sounds, both lasting half a second. Cond Tone is followed by an air puff delivered to the animals' face following a half-second delay. UC Puff is an identical air puff without any preceding tone. (C) Spike rates are stable during maintenance dose. Average firing rates (1-min bins) displayed for each brain area (mean ± *SEM*). Horizontal black bars (top) indicate the time course of propofol infusion dosage. A high dose was given for 30 min (onset) followed by 30 min of a lower dose (maintenance). Purple bars mark the average time for LOC and recovery of consciousness (ROC). Time ranges used for Awake and Unconscious states are indicated by gray boxes.

Data Analysis

Spectral Analysis

All spectrograms were computed using 400-msec length windows with 50-msec step sizes. We used multitaper spectral estimation to improve power spectral density estimation (Babadi & Brown, 2014). The number of tapers were selected using floor($2TW - 1$) tapers, where T is the length of the window in seconds and W is the half-bandwidth of our desired spectral resolution. We used $W = 4$, which resulted in two tapers.

Average spectrograms for each brain area were computed across electrodes and trials for a given session. Reported averages were then calculated across sessions. Spectrograms are reported as total power (Cohen, 2014). To display the change in power related to stimulus presentation, baseline power was calculated using 500–200 msec before the stimulus was given. The change from baseline was then calculated as:

$$\Delta\text{dB} = 10\log\left(\frac{\text{power}}{\text{baseline power}}\right)$$

Two different measures were used for quantifying synchronization between brain areas. Coherence, which measures the across-trial correlation in phase-offset and amplitude between electrodes, was calculated for each frequency ω as described in Kramer and Eden (2016):

$$\text{coh}(\omega) = \frac{\frac{1}{N}\sum_{n=1}^{N}\left|S_{xy}^{n}(\omega)\right|}{\sqrt{\frac{1}{N}\sum_{n=1}^{N}S_{xx}^{n}(\omega)\frac{1}{N}\sum_{n=1}^{N}S_{yy}^{n}(\omega)}}$$

where N is the number of trials; S_{xx}^{n} and S_{yy}^{n} are the power on trial n for signal x and y, respectively; and S_{xy}^{n} is the cross-spectrum on trial n. The phase-locking value (PLV) is designed to capture consistent phase relationships between signals without any effect of signal amplitude (Lachaux, Rodriguez, Martinerie, & Varela, 1999). Letting $\phi_{x}^{n}(\omega)$ be the phase of signal x and $\phi_{y}^{n}(\omega)$ be the phase of signal y on trial n, the PLV for frequency ω is then:

$$\text{PLV}(\omega) = \left|\frac{1}{N}\sum_{n=1}^{N}e^{i\left(\phi_{x}^{n}(\omega)-\phi_{y}^{n}(\omega)\right)}\right|.$$

The average coherence or PLV reported for each brain area pair was found by taking the average coherence across all pairs of electrodes from the two areas. Baseline normalization was performed by subtracting the average baseline coherence value (500–200 msec before stimulus). PLV was averaged and baseline-normalized similarly. Non-phase-locked (induced) coherence and PLV were calculated by subtracting the trial-averaged time domain response from each trial before computing the frequency response. All spectrograms and synchrony measures were computed using the Spynal Python library (Brincat, 2023).

Stimulus Decoding

Stimulus decoding was performed using LFP data and the UC Tone, UC Puff, and Cond Tone stimuli. Stimulus trial data were first binned in 20-msec intervals. For each 20-msec bin, the population data were "flattened" by

concatenating timepoints. That is, a matrix of size (electrodes, time) would be transformed to an array of length (electrodes × time). This method was chosen to retain all available information. For each bin of data, we used a linear support vector classifier (SVC in Python's sklearn package (Pedregosa et al., 2011), with default regularization parameter $C = 1$) for decoding analysis, which was performed separately on each experimental session (Hastie, Tibshirani, & Friedman, 2009; Cortes & Vapnik, 1995). For a given session, a decoder was trained on labeled data (UC Tone, UC Puff, and Cond Tone) from a given time bin. Accuracy was then assessed on held out test data. Average test accuracy from a 10-fold cross-validation was calculated for each session. (That is, we held out a test set containing 10 percent of trials and trained on the remaining 90 percent of the data.) The session test accuracy was computed by repeating this process of 10 non-overlapping test sets that partitioned the data and taking the average test accuracy. The final reported means and standard errors were then calculated using the test accuracies from each session.

Statistical Analysis

Statistical tests for changes in coherence were performed by first transforming the values to be normally distributed and then using standard t tests (Jarvis & Mitra, 2001). Nonparametric tests (Wilcoxon) were used for all other statistical comparisons (one-sample for stimulus vs. baseline, two-sample for Awake vs. Unconscious). Multiple comparison corrections were performed using false discovery rate correction with a family-wide error rate of 0.01 (Seabold & Perktold, 2010).

Hidden Markov Model for Estimating Spiking Responses

Model Specification

To account for the presence of Up and Down states in the Unconscious state, we designed a Hidden Markov Model (HMM) to estimate spiking stimulus responses (Rabiner, 1989; summarized in Figure 2). Before introducing the formal structure of the model, we provide a brief conceptual description. Each neuron has two mean firing rate

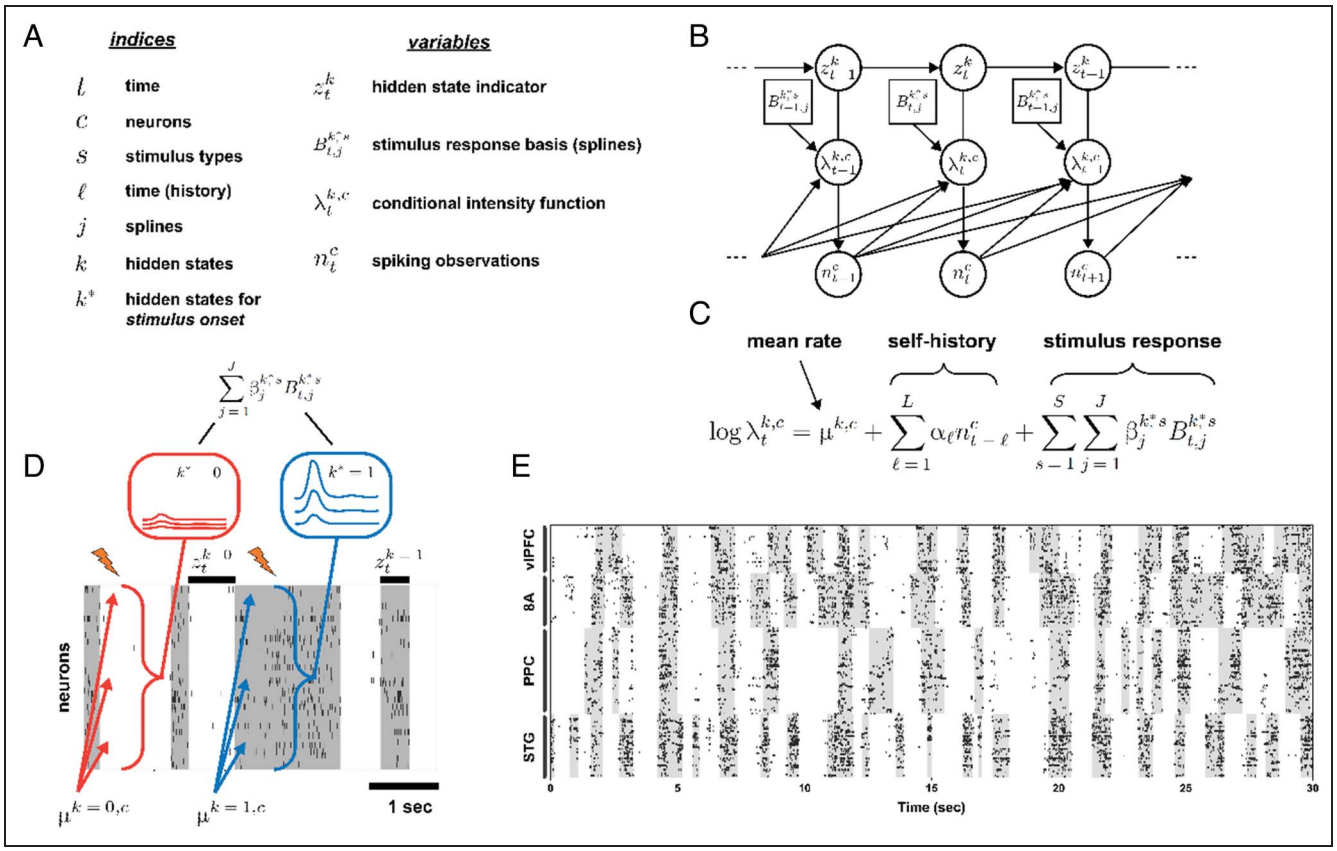

Figure 2. HMM used for estimating spiking stimulus responses in the Unconscious state. (A) Model notation. (B) Graphical model structure of the HMM. (C) The CIF for a neuron in the model. Each neuron has a distinct mean rate parameter that differs between Up and Down states. Self-history and stimulus response parameters are shared across neurons. (D) Stimulus response schematic. In the Down state, neurons hypothetically will have a low firing rate (red arrows) and minimally respond to the stimulus (red box). In Up states, baseline firing rates increase (blue arrows), and stimulus response is heightened (blue box). (E) Raster plot showing 30 sec of spiking data from NHP 1 during the Unconscious state. Up and Down spiking states are visible in each brain area. Gray boxes indicate Up state labels produced by the HMM algorithm.

parameters, one for Up states and one for Down states (Figure 2A–D). In the absence of a stimulus, each neuron's firing rate is a function of the mean rate parameters, the hidden state (Up or Down), and the neuron's spiking history (Figure 2C). Finally, the stimulus response is modeled using a spline basis and separate sets of coefficients depending on which state stimulus onset occurs in (Figure 2C–D). We are interested in quantifying the average response across neurons within a given brain area, and thus the parameters governing the stimulus response are shared across neurons.

Let $k \in \{0, \ldots, K\}$ be the discrete states in the system. In the analysis of spiking responses in the Unconscious state, we let $K = 2$ with $k = 1$ and $k = 0$ representing the Up and Down states, respectively. Next, we define an indicator function z_t^k, which equals 1 if the system is in state k and 0 otherwise. Let $\boldsymbol{z}_t = \left(z_t^1, \ldots, z_t^K\right)$ refer to the vector of indicator functions for all hidden states. The state transition probabilities are represented in a state transition matrix:

$$\mathbf{A}_{j,k} = P\left(z_t^k = 1 | z_{t-1}^j = 1\right) \tag{1}$$

which is treated as an unknown parameter to be estimated. We use $\boldsymbol{\pi}$ to denote the initial state probabilities.

The spiking observations for neuron $c \in \{1, \ldots, C\}$ are modeled as a point process (Kass, Ventura, & Brown, 2005; Daley & Vere-Jones, 2003). Letting $N_{(a,b]}^c$ denote the number of spikes occurring in the time range $(a, b]$ for $a < b$ and H_t^c denote the history of the process Up to time t, the conditional intensity function (CIF) for neuron c is defined as:

$$\lim_{\Delta \to 0} \frac{P\left(N_{(t,t+\Delta]}^c = 1 \mid \boldsymbol{z}_t, H_t^c\right)}{\Delta} = \lambda_t^c \tag{2}$$

where Δ is the time-bin width and $H_t^c = \left(n_{t-1}^c, \ldots, n_{t-L}^c\right)^\top$ is the neurons self-history for time lag $\ell \in \{1, \ldots, L\}$. We assume that for a small Δ (typically 1 msec as in our study), we can make an accurate discrete-time approximation to the continuous-time CIF at time t as

$$P\left(n_t^c = 1 | \boldsymbol{z}_t, H_t^c\right) = \lambda_t^c \Delta \tag{3}$$

where $\lambda_t^c \Delta$ is linked to the hidden states by:

$$\lambda_t^c = \prod_{k=1}^{K} \left(\lambda_t^{k,c}\right)^{z_t^k} \tag{4}$$

Next, let $s \in \{1, \ldots, S\}$ represent the different stimulus types (e.g., UC Tone). We define the CIF for each state k to be a function of a mean rate, spiking history, and the sensory stimulus:

$$\log \lambda_t^{k,c} = \mu^{k,c} + \sum_{\ell=1}^{L} \alpha_\ell n_{t-\ell}^c + \sum_{s=1}^{S} \sum_{j=1}^{J} \beta_j^{k^*,s} B_{t,j}^{k^*,s} \tag{5}$$

where we have history coefficients $(\alpha_1, \ldots, \alpha_L)^\top$, $s \in \{1, \ldots, S\}$ is the stimulus type, k^* is the hidden state in which stimulus onset occurred, and the $B_{t,j}^{k^*,s}$ serves as a basis for modeling the stimulus response. We note that the history terms create conditional dependencies across observations over time, which is not standard in HMMs. However, because these dependencies occur in the observation equation, no major changes to the estimation algorithm are required (this structure is commonly seen in autoregressive HMMs; Murphy, 2023; Hamilton, 1990).

We model the stimulus response with parameters shared across neurons, rather than modeling response parameters for each neuron individually, for two reasons: First, as we cannot ensure identical neuron populations are recorded in each session, we target a mean population response that can be easily combined across sessions. Second, limited stimulus response data per session might preclude reliable individual parameter estimates for each neuron. Although we acknowledge this is an oversimplification biophysically, we argue that a model estimating a mean population response in each area, alongside individual mean firing rates, strikes a balanced compromise between accuracy and practicality, and is sufficient for our study's research questions.

Expectation Maximization Algorithm

Given the observed spiking data, our objective is to estimate the parameters:

$$\boldsymbol{\theta} = \left\{\pi^k, \mathbf{A}, \mu^{k,c}, \alpha_\ell, \beta_j^{k^*,s}, k^*\right\}_{k=1,c=1,\ell=1,j=1,s=1}^{K,C,L,J,S} \tag{6}$$

We estimate the parameters and hidden states using the expectation maximization (EM) algorithm (Dempster, Laird, & Rubin, 1977), a standard approach for HMMs and latent variable models more generally (Murphy, 2023; Bishop, 2006). The EM algorithm works by iterating between (1) taking the expected value of the complete-data log likelihood with respect the conditional distribution of the hidden states given the data and (2) maximizing the expected complete-data log likelihood over $\boldsymbol{\theta}$. We define the Q-function $Q(\boldsymbol{\theta}|\boldsymbol{\theta}^{(r)})$ as the expectation of the complete-data log likelihood, on iteration $r + 1$ of the EM algorithm, using the parameters $\boldsymbol{\theta}^{(r)}$ from the previous iteration.

E-Step. In the E-Step, the conditional distribution of the hidden states given the observed data is computed. We use the standard approach of the forward–backward algorithm and refer the reader to Murphy (2023), Bishop (2006), and Rabiner (1989) for details.

M-Step. In the M-Step, we maximize $\boldsymbol{\theta}$ in the Q-function. The state parameters $\boldsymbol{\pi}$ and $\mathbf{A}$ have standard closed form solutions. Closed form solutions do not exist for the point process parameters, and they must be found numerically.

We use the Broyden-Fletcher-Goldfarb-Shanno algorithm (Virtanen et al., 2020; Fletcher, 2013) for this purpose. Finally, after updating the other parameters, we run the Viterbi algorithm to determine the most likely state path, which is used to update the k^* assignments.

In preliminary work, we found that the Up and Down state labels produced by our model switched between states too frequently, likely because of the high time resolution and binary nature of the data. We found that the labels were improved by putting a Dirichlet prior distribution on the $\mathbf{A}$ matrix to favor self-transition (i.e., higher probabilities along the diagonal) (Linderman, Antin, Zoltowski, & Glaser, 2020). Specifically, denoting the j^{th} row of the matrix $\mathbf{A}$ as $\mathbf{A}_{j,1:K}$, we put a prior distribution on each row:

$$\mathbf{A}^{(\mathbf{r})}{}_{j,1:K} \sim \text{Dirichlet}\left(\boldsymbol{\phi}_j\right) \tag{7}$$

where

$$\boldsymbol{\phi}_j = \left(\phi_{j,1}, \ldots, \phi_{j,K}\right)$$

The same parameters values are used for each row, adjusting for the position of the row entry that corresponds to the diagonal element of $\mathbf{A}$. Noting that the Dirichlet distribution is the conjugate prior for the categorical distribution, the closed-form parameter update is (Murphy, 2023):

$$\mathbf{A}^{(r+1)}{}_{j,k} = \frac{c_{j,k} + \phi_{j,k} - 1}{\sum_{k=1}^{K}\left(c_{j,k} + \phi_{j,k} - 1\right)} \tag{8}$$

using

$$c_{j,k} = \sum_{t=2}^{T} \mathrm{E}\left[z^j_{t-1} z^k_t\right].$$

Estimated Stimulus Response and Confidence Intervals

For visualization purposes (Figure 6), we defined an estimated stimulus response summary across all neurons for a session:

$$\log \widehat{\lambda^{k,s}_t} = \widehat{\mu^k} + \sum_{j=1}^{J} \widehat{\beta^{k^*,s}_j} B_{t,j} \tag{9}$$

where

$$\widehat{\mu^k} = \frac{1}{C}\sum_{c=1}^{C} \widehat{\mu^{k,c}}$$

The variance of parameter estimates was calculated using the method of Louis (1982), which enables calculating the observed Fisher information when using the EM algorithm to produce maximum likelihood estimates (Efron & Hinkley, 1978). On some sessions, we found that the variance of a small number (fewer than 10 percent of neurons) of the $\mu^{k,c}$ parameters were very high. These neurons typically showed very low firing rates and were removed for the calculation of the stimulus response. Confidence intervals were then calculated using the delta method (Cramér, 1999; Doob, 1935). Further details on parameter estimation and confidence intervals are provided in Appendix B.

We combined session-level results and uncertainty by taking an average of the parameter estimates across sessions. Within sessions, the $\mu^{k,c}$ were assumed to be independent from each other and from the $\beta^{k^*,s}_j$ parameters. Following the asymptotic normality of maximum likelihood estimators, we assume the parameter estimates from each session are Gaussian distributed and combined estimates across sessions following the properties of summation for Gaussian random variables (Pawitan, 2001; Sweeting, 1980).

Implementation

We implemented our model as a custom observation class in the SSM package (Linderman et al., 2020). We first applied a Poisson HMM to the data and used the fitted values to initialize $\boldsymbol{\pi}$,$\mathbf{A}$ and the $\mu^{k,c}$ parameters in our model. The α_ℓ and $\beta^{k^*,s}_j$ parameters were initialized at 0. We applied the HMM to spiking data during the Unconscious state, which contained Up and Down states. We used a value of 1×10^{12} for the "diagonal component" of $\boldsymbol{\phi}_j$ for NHP 1 in all brain areas and 1×10^8 for vlPFC in NHP 2. The off-diagonal elements of $\boldsymbol{\phi}_j$ were set to 1, and the row was then normalized to sum to one (Linderman et al., 2020). A separate model instance was used to estimate the Awake response using $K = 1$ (i.e., constant hidden state). In this case, the EM algorithm is not needed. Rather, the parameter estimation described in the M-Step above is simply performed once.

For self-history, we used $L = 10$ to account for refractory periods. For the stimulus response basis $B^{k^*,s}_{t,j}$, we used natural cubic splines with knots spaced 50 msec apart (Bartels, Beatty, & Barsky, 1995; Wegman & Wright, 1983). This basis used $J = 24$ and spanned from 200 msec before stimulus to 1000 msec after stimulus. To ensure that the basis functions were non-overlapping across stimulus types, we started the basis for the Cond Puff at stimulus presentation time, resulting in $J = 20$. When plotting the estimated response for the Cond Puff, we used the $\beta^{k^*,s}_j$ parameters from the end of the Cond Tone estimated response that occupied the 200 msec preceding the Cond Puff stimulus.

RESULTS

We administered propofol to two NHPs. Twenty-one experimental sessions were performed (11 sessions NHP 1, 10 sessions NHP 2). They were first given a high dose of propofol (285–580 μg/kg/min) for 30 min to induce LOC. This was followed by 30 min of a lower maintenance dose (70–320 μg/kg/min), similar to that used to maintain

anesthesia in human surgeries (see Methods section for details about propofol administration). LFP and spiking were recorded simultaneously from Utah arrays implanted in four cortical areas: STG, a secondary auditory center; PPC, an associative region; 8A and vlPFC, cognitive areas of prefrontal cortex (Figure 1A).

Three different stimuli were presented to the NHPs throughout each session to characterize sensory processing under anesthesia (see Methods section). One was a puff of air to the face. As in our previous study, the lack of behavioral response to the airpuff, along with other measures such as eyes opening and closing, was used to determine loss and subsequent recovery of consciousness (see Methods section). We also presented two distinct brief (500 msec) auditory tones (Figure 1B). One tone always preceded an airpuff by 500 msec. We call this the Cond Tone. A second tone (UC Tone) was always presented alone. We also presented airpuffs alone without any preceding tone (UC Puff). Although these stimuli were designed with a conditioning component, we did not investigate the effect of propofol on conditioned responses, focusing instead on propofol's general impact on sensory responses across cortex. Nonetheless, all the stimuli are included in our analyses, and we use their original nomenclature for completeness. We also note that we cannot rule out that the NHPs were dreaming, which has been shown to occur during propofol anesthesia in humans and is a form of consciousness (Valli et al., 2023; Leslie et al., 2009). We thus limit our definition of unconsciousness in this study to the loss of Awake-like behavior (eyes closed and no response to airpuff), which is commonly used in the field (Tasserie et al., 2022; Redinbaugh et al., 2020; Ma, Liu, & Hudson, 2019; Ishizawa et al., 2016; Liu et al., 2015).

Anesthesia Alters Cortical Responses to Sensory Stimuli

Cortical responses to stimuli were altered during the Unconscious state relative to the Awake state. We compared LFP spectral power in the Awake versus Unconscious states (Figure 3). During the Awake state, the Cond Tone, Cond Puff, and UC Puff evoked an increase in power (relative to prestimulus baseline; see Methods section) in the alpha–beta (8–25 Hz) band for all cortical areas (Figure 3B–C, contour lines indicate $p < .05$, Wilcoxon). During the Awake state, the STG also showed a broadband increase in higher frequency power (> 30 Hz) to all stimuli (Figure 3A–C). The higher frequency response was weaker in the higher cortical areas. The UC Tone elicited weaker responses than the Cond Tone, Cond Puff, and the UC Puff (Figure 3A, contour lines indicate $p < .05$, Wilcoxon). During the Unconscious state, the alpha–beta response was decreased in STG and virtually disappeared in the higher cortical areas (Figure 3B–C). In STG (but not other areas), there was an increase in the higher frequency broadband response to the Cond Tone, UC Tone, and UC Puff (but not the Cond Puff) relative to the Awake state (Figure 3A–C).

Stimulus Information Is Progressively Lost through the Cortical Hierarchy during Unconsciousness

Next, we turn to measures of stimulus information. We used a linear classifier to decode stimulus identity using LFP data (see Methods section for details). To isolate the activity to individual stimuli, we looked at decoding for stimuli for which there was no immediately preceding stimulus (i.e., UC Tone, Cond Tone, and UC Puff).

During the Awake state, stimulus information was found in all regions of cortex (Figure 4A). During the Unconscious state, stimulus information showed a significant decrease in all areas, as measured by change in the maximum decoding performance achieved during a 50- to 250-msec poststimulus time range (Figure 4B; Wilcoxon; $p < .001$). In STG, the decrease in stimulus information was relatively modest. Classifier decoding remained well above chance (Figure 4A; Wilcoxon; $p < .001$). This suggests that a significant amount of stimulus information still reaches intermediate-level sensory cortex. By contrast, in the Unconscious state, stimulus information progressively decreased across areas and was near chance levels in vlPFC, relative to the Awake state.

Inter-area Synchronization Is Disrupted during Anesthesia

Our results suggest that propofol anesthesia disrupts feedforward transmission of sensory information from sensory (e.g., STG) to higher cortical areas (e.g., PPC, vlPFC, 8A). One potential explanation is decreased communication between the areas. Oscillatory synchronization is thought to underlie such communication (Kramer & Eden, 2016; Kass, Eden, & Brown, 2014; Fries, 2005; Singer, 1993). Thus, we looked for evidence of altered patterns of LFP synchronization during the Unconscious state. We measured stimulus-related synchronization as either "induced," meaning the trial-averaged (evoked) response was subtracted from individual trials in the time-domain, or "total," in which the evoked response was not subtracted from each trial (Cohen, 2014; David, Kilner, & Friston, 2006). We quantified synchronization with PLV and coherence, two measures of phase-offset consistency between signals (see Methods section for details). Figure 5 displays results for induced PLV. Figures A1–A3 show results for the other synchronization measures.

During the Awake state, we found significant stimulus-related alpha–beta synchrony between 8A-vlPFC for the UC Puff and Cond Tone stimuli (Figure 5B–C, contour lines indicate $p < .05$, Wilcoxon). Stimulus-related synchrony was also observed in the Awake state in response to the UC Puff stimuli within the alpha and low-beta frequency bands for all area pairs except PPC-vlPFC and STG-vlPFC, as well as in response to Cond Tone/Cond Puff

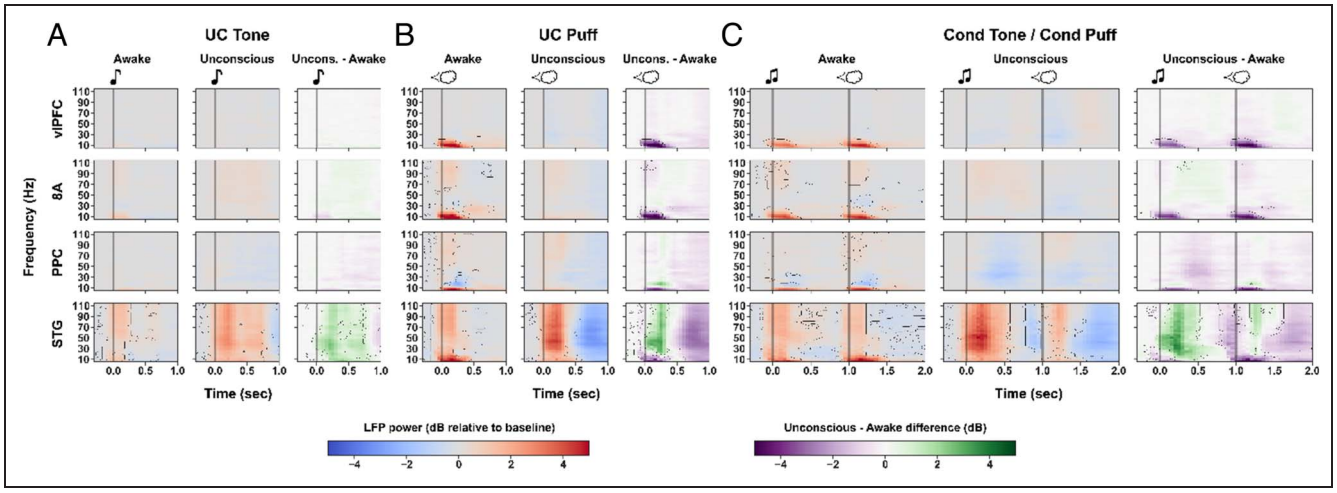

Figure 3. Alpha–beta frequency range responses are lost in higher order cortical areas during anesthesia. (A–C) Change in time–frequency power relative to prestimulus baseline in Awake and Unconscious state for each stimulus. Vertical gray bar indicates stimulus onset time. The rightmost part for each stimulus shows the difference in power between Awake and Unconscious responses. Contour lines show regions of statistical significance (Wilcoxon test with false discovery rate correction for multiple comparisons). Stimulus-induced alpha–beta responses disappear during anesthesia, especially in the higher level cortical areas. Area STG also shows an increase in higher frequency power relative to baseline under propofol.

stimuli for PPC-vlPFC and PPC-8A (Figure 5B–C, contour lines indicate $p < .05$, Wilcoxon). No stimulus-related synchrony was observed for the UC Tone in the Awake state (Figure 5A). During the Unconscious state, there was little or no stimulus-related synchrony for any of the pairs of cortical areas to any of the stimuli (Figure 5A–C). Similar results were also found using induced coherence as a measure of synchrony (Figure A1). Total PLV and coherence showed a similar trend, with stronger synchrony in the Awake state (Figures A2–A3).

Stimulus Responses during Spiking Up States Are Not Awake-like

Next, we examined the spiking response to sensory stimulation. Previous work has shown propofol anesthesia

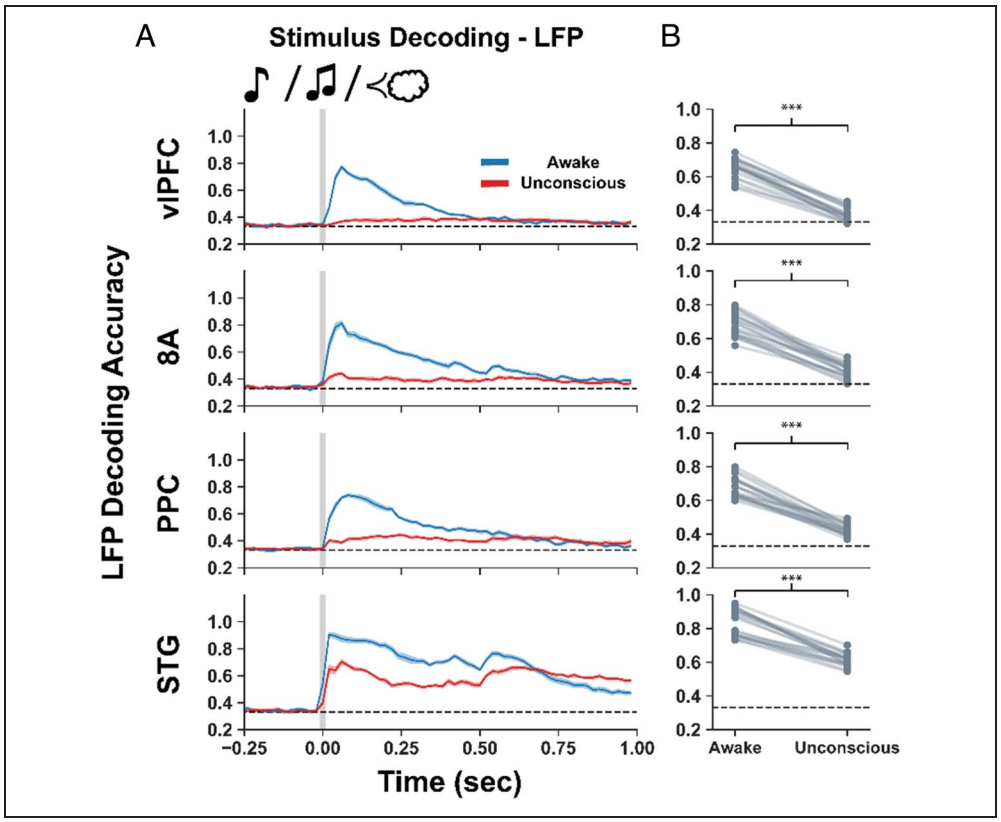

Figure 4. Stimulus information is lost progressively through cortical hierarchy during anesthesia. (A) Decoding accuracy between the UC Tone, UC Puff, and Cond Tone stimuli on LFP in each cortical area. Shaded region represents ± *SEM*. (B) Change in average decoding accuracy between 50 and 250 msec poststimulus for each experimental session. Significance markers indicate difference between Awake and Unconscious (Wilcoxon; $p < .001$).

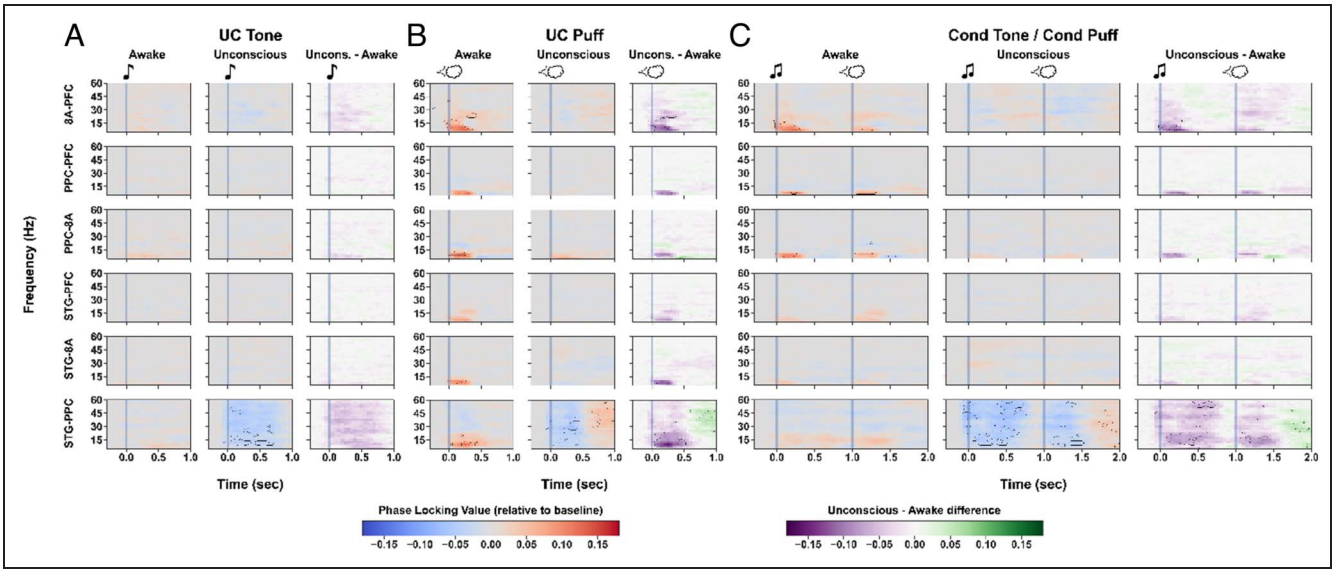

Figure 5. Propofol eliminates stimulus-related synchronization between cortical areas. Synchronization was calculated using PLV (see Methods section). (A–C) Stimulus-related change from baseline synchrony in Awake (left) and unconscious (middle) for indicated stimuli. The right column shows the difference between Unconscious and Awake. Contour lines show regions of statistical significance (Wilcoxon). Sensory stimulus-related alpha–beta synchronization observed between cortical areas in the Awake state is largely lost during propofol anesthesia.

creates alternating periods of high and low spiking activity referred to, respectively, as Up and Down states (Bastos et al., 2021; Lewis et al., 2012). This raised the possibility that cortical signal transmission might only be impaired during Down states and relatively preserved during Up states. Because standard methods relying on linearity, independence, and identical trials are inadequate in this context, we followed a

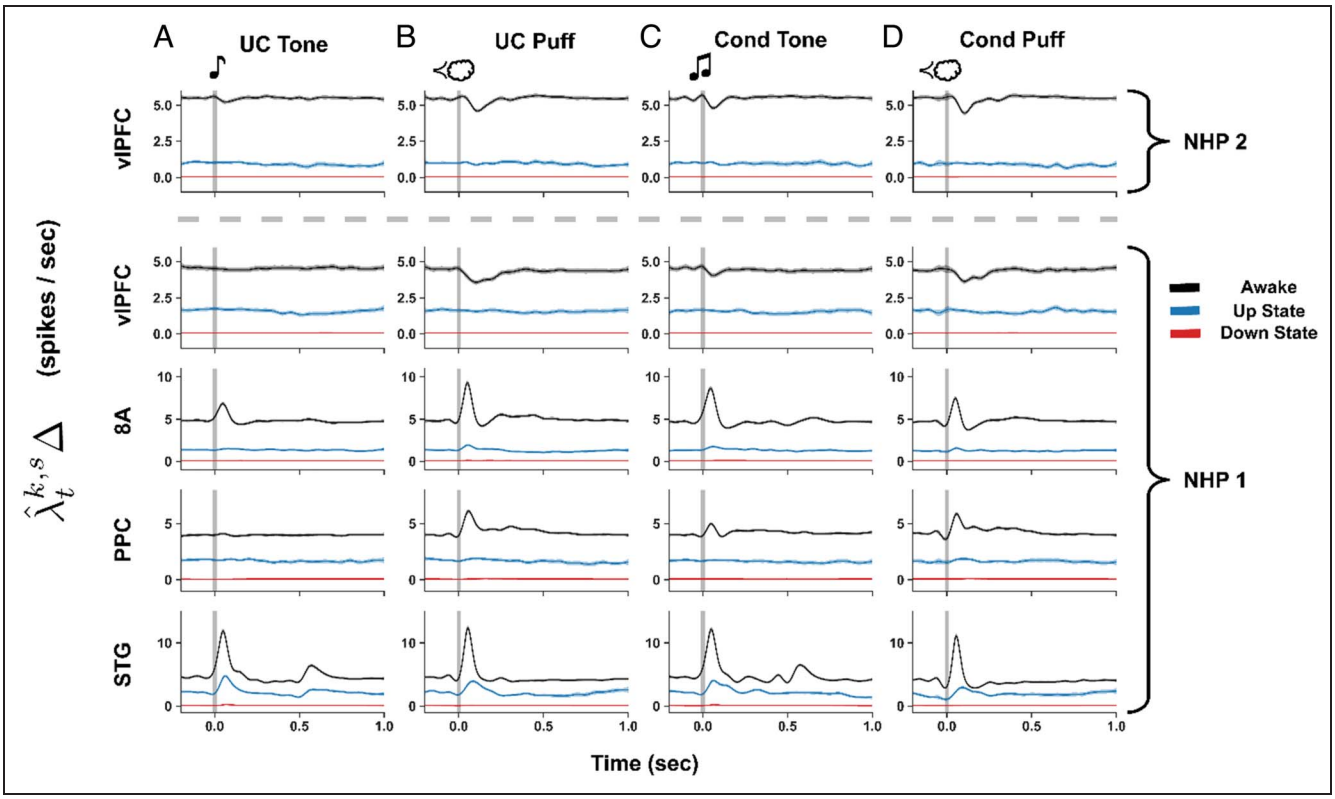

Figure 6. (A–D) Estimated population spiking responses to sensory stimuli for Awake (black), Down states (red), and Up states (blue) during unconsciousness. For NHP 2, estimated responses are only reported for vlPFC (see Methods section). Shaded regions show 95% confidence intervals.

model-based time-series approach to estimate stimulus responses.

HMMs are widely used in statistics and machine learning to model time-series data that alternates between discrete underlying "states" (Cajigas et al., 2021; Garwood et al., 2021; Song et al., 2019; Chen, Vijayan, Barbieri, Wilson, & Brown, 2009; Rabiner, 1989). We designed and applied an HMM to simultaneously (1) label Up and Down states and (2) estimate an average stimulus response within an area, taking account of the Up and Down states (see Methods section for details). Although LFP data quality and results were consistent across animals, spike recordings in NHP 2 suffered from complications (see Methods section). For this reason, spiking responses for NHP 2 are only reported for vlPFC. We found the average duration of Up states produced by the model was 0.97 ± 0.09 sec for STG, 0.89 ± 0.06 sec for PPC, 2.07 ± 0.37 sec for FEF, 1.13 ± 0.10 sec for vlPFC of NHP1, and 0.69 ± 0.06 sec for vlPFC of NHP2. The average duration of the Down states was 0.86 ± 0.06 sec for STG, 0.79 ± 0.06 sec for PPC, 1.18 ± 0.10 sec for FEF, 0.97 ± 0.4 sec for vlPFC of NHP1, and 0.70 ± 0.07 sec for vlPFC of NHP2. These are in line with Up and Down state durations described previously as being between light and deep anesthesia (Torao-Angosto, Manasanch, Mattia, & Sanchez-Vives, 2021). We also note Up states showed reduced baseline firing rates compared with the Awake state in all areas (Figure 6A–D).

We found that during the Awake state in NHP 1, there were spiking responses to all stimuli in STG and 8A (Figure 6A–D, shaded regions display 95% CIs). The PPC did not show a spiking response to the UC Tone whereas the other stimuli elicited excitatory responses. The vlPFC showed a decrease in spiking in both NHPs to the Cond Tone and the airpuffs, but not the UC Tone (Figure 6A–D). By contrast, in the Unconscious state, responses were drastically reduced. All areas showed minimal spiking to stimuli occurring during Down states. Stimuli that occurred during Up states in STG of NHP 1 evoked responses similar to that observed in the Awake state, but with reduced baseline and maximum firing rates (Figure 6A–D). In PPC and 8A of NHP 1, stimuli occurring in Up states were either absent or dramatically reduced compared with the Awake state (Figure 6A–D). The vlPFC of both animals did not show spiking responses to stimuli occurring in Up states (Figure 6A–D).

DISCUSSION

We found that in the Unconscious state, auditory cortex neural responses to sensory stimuli persisted. However, in higher order cortex, information was progressively lost. In the Awake state, stimulus information was present at all levels of cortex (auditory, parietal, and prefrontal). In the Unconscious state, there was a modest reduction of stimulus information in auditory cortex. In parietal cortex and 8A (frontal cortex), information was greatly reduced. In vlPFC, stimulus information was reduced to near zero. This could have been because of a breakdown in cortical communication. Stimulus-related alpha–beta synchronization between areas was evident in the Awake state. However, this synchronization disappeared in the Unconscious state. Finally, disruption of sensory processing in the Unconscious state consisted of Down states with highly sparse spiking and Up states in which sensory stimulus responses persisted in auditory cortex. Stimulus responses seen in higher order brain areas in the Awake state were largely lost in Unconscious state.

Many previous studies have examined overall neural state changes because of propofol anesthesia. These changes include an increase in slow-frequency cortical oscillations, a decrease in spiking and high-frequency activity, and a shift of alpha–beta oscillations from posterior to frontal cortex (Bastos et al., 2021; Redinbaugh et al., 2020; Lewis et al., 2015; Purdon et al., 2013; Vijayan, Ching, Purdon, Brown, & Kopell, 2013; Lewis et al., 2012; Ching, Cimenser, Purdon, Brown, & Kopell, 2010). Propofol's effect on sensory processing is less well understood but has been investigated previously (Krom et al., 2020; Banks et al., 2018; Nourski et al., 2017, Ishizawa et al., 2016; Liu et al., 2012; Supp, Siegel, Hipp, & Engel, 2011). Broadly, these studies reported results in line with ours, namely, persistent but altered stimulus responses in sensory cortex. It is worth noting one study in rodents found that alterations of sensory responses and information in auditory cortex occurred before behavioral changes that reflect LOC, so this may not be a necessary condition for unconsciousness (Banks et al., 2018).

In humans, previous studies have also found differential effects of propofol on sensory and higher order cortex (Nourski et al., 2017, 2018, 2021; Liu, Lauer, Ward, Li, & Hudetz, 2013; Liu et al., 2012; Heinke et al., 2004). A recent study using intracranial electrodes in humans found weaker spiking to auditory stimuli in associative cortex but a relative preservation in auditory cortex (Krom et al., 2020). A human EEG study attributed the loss of sensory responses in higher cortex to increased alpha synchronization in frontal cortex (Supp et al., 2011). In NHPs, Ishizawa and colleagues (2016) also found that spiking responses to sensory inputs persisted in sensorimotor cortex but were reduced in the higher order premotor area. Our study confirms and expands these observations to additional cortical areas. Under propofol-mediated unconsciousness, we found that stimulus-induced interarea alpha–beta synchronization disappeared. Previous studies in humans have provided divergent results on propofol's effect on functional connectivity, with both decreases (Lee et al., 2013; Boly et al., 2012; Boveroux et al., 2010) and increases (Banks et al., 2020; Lee et al., 2017; Monti et al., 2013) being reported. Increased functional connectivity was also found in the oculomotor circuit of NHPs (Ma et al., 2019). These studies measured functional connectivity in the absence of sensory stimuli,

whereas in our study, we found propofol-mediated unconsciousness disrupted stimulus-related communication by looking at sensory information directly. Nonetheless, the effect of propofol on general inter-area synchronization appears to be complex and area dependent. How propofol impacts the circuits involved in communicating sensory information is likely complex as well. The loss of stimulus-related alpha–beta synchronization we observed suggests an impact on top–down feedback may be part of the picture (Bastos et al., 2015; Liu et al., 2015; van Kerkoerle et al., 2014).

Propofol anesthesia broadly causes an increase in low-frequency power (the slow-wave and alpha rhythm) and a decrease in high-frequency power in cortical LFP and EEG recordings (Bastos et al., 2021; Purdon et al., 2013). Thus, it was surprising to find that, in auditory cortex, propofol enhanced stimulus-related broadband power (across all observed frequencies 10–110 Hz). The spectral peak of this effect was in the lower gamma band (30–60 Hz). Previous studies in humans with a variety of stimulus types, recording modalities, and sensory areas have shown both increased (Krom et al., 2020; Saxena et al., 2013) and decreased (Nourski et al., 2017, 2018, 2021) stimulus-related, high-frequency power during propofol anesthesia. Future studies will be needed to clarify how propofol modulates high-frequency power in different sensory contexts. We note that given our observation that propofol decreased stimulus-related spiking activity in STG, the increase in broadband power we observed cannot be attributed to an increase in spiking activity (Ray & Maunsell, 2011). One possible explanation for this decoupling of stimulus-related broadband power and spiking is subthreshold synaptic effects (Miller, Honey, Hermes, Rao, & Ojemann, 2014; Buzsáki, Anastassiou, & Koch, 2012).

During propofol-mediated unconsciousness, spiking couples to the phase of the slow wave (0.1–4 Hz; Bastos et al., 2021; Lewis et al., 2012). The results are Down states with little spiking alternating with Up states with increased spiking (Bastos et al., 2021). In theory, propofol-induced disruption of sensory processing could be due only to the Down states (Camassa, Galluzzi, Mattia, & Sanchez-Vives, 2022) and Up states could be small temporal "islands" of normal processing, as has been proposed in sleep (Destexhe, Hughes, Rudolph, & Crunelli, 2007). However, our results did not support that. We found sensory stimuli elicited spiking responses in auditory cortex during Up states that were reduced compared with responses in the Awake state. In higher order cortical areas, spiking responses observed in the Awake state were dramatically reduced or absent in Up states. This suggests that Up states do not represent short recapitulations of normal conscious activity but rather are a neurophysiologically distinct state.

Our results are consistent with findings of stimulus responses occurring during Up states in other anesthetics and in other sensory modalities. In the visual cortex of cats under a variety of anesthetics, sensory stimuli trigger enhanced responses during Up states compared with Down states (Haider, Duque, Hasenstaub, Yu, & McCormick, 2007; Azouz & Gray, 1999; Arieli, Sterkin, Grinvald, & Aertsen, 1996). In the whisker barrel (somatosensory) cortex of rodents under anesthesia, synaptic sensory responses and spiking have been reported as suppressed in Up states compared with Down states (Sachdev, Ebner, & Wilson, 2004; Petersen, Hahn, Mehta, Grinvald, & Sakmann, 2003), but other groups have found increased spiking responsiveness and stimulus information during Up states (Alenda, Molano-Mazón, Panzeri, & Maravall, 2010; Rigas & Castro-Alamancos, 2007). One group found a stimulus-intensity dependent effect (Reig, Zerlaut, Vergara, Destexhe, & Sanchez-Vives, 2015). Intriguingly, sensory stimuli have been shown to trigger Up states when they occur in Down states in the whisker barrel cortex (Hasenstaub, Sachdev, & McCormick, 2007; Reig & Sanchez-Vives, 2007). In our study, we focused on what happens when stimuli occur during Up states and did not account for the possibility that sensory input could trigger an Up state in our HMM model. Future studies in NHPs and humans should investigate whether this phenomenon is limited to the barrel cortex of rodents or is more general.

Although the neurophysiological states of sleep and anesthesia are distinct (Zelmann et al., 2023; Moody et al., 2021; Akeju & Brown, 2017), both do share slow wave oscillations and Up and Down states of spiking (Hoffman et al., 2007; Steriade, Timofeev, & Grenier, 2001; Steriade, McCormick, & Sejnowski, 1993). As in our study, stimulus responses have shown to be preserved in auditory cortex during sleep in rodents (Sela, Vyazovskiy, Cirelli, Tononi, & Nir, 2016), NHPs (Issa & Wang, 2011), and humans (Hayat et al., 2022). There is evidence, however, that sensory processing is conserved beyond sensory cortical areas in sleep (Andrillon & Kouider, 2020; Andrillon, Poulsen, Hansen, Léger, & Kouider, 2016) and a recent study found that the slow wave dynamics and Up and Down states in anesthesia are less sensitive to external inputs compared with Up and Down states in sleep (Nghiem et al., 2020). We found sensory processing to be severely limited beyond auditory cortex, suggesting a differential impact on sensory processing in sleep and anesthesia.

Several hypotheses have been proposed to explain disruption of sensory processing during anesthetic-induced unconsciousness. The "thalamic gating" hypothesis suggests sensory processing is disrupted at the level of the thalamic relay to primary sensory cortex (Alkire, Haier, & Fallon, 2000). Our results, along with others (Filipchuk, Schwenkgrub, Destexhe, & Bathellier, 2022; Raz et al., 2014; Supp et al., 2011; Boveroux et al., 2010; Davis et al., 2007; Imas, Ropella, Ward, Wood, & Hudetz, 2005; Heinke et al., 2004), instead suggest neural responses in sensory cortex, and thus thalamocortical sensory relay connections, are largely preserved. However,

thalamocortical connections do more than just relay sensory information. Higher order thalamocortical circuits are known to be important for many cognitive functions and likely play an important role in consciousness (Müller et al., 2023; Cosgrove et al., 2022; Mofakham et al., 2021, 2022; Schmitt et al., 2017). Our findings are thus in line with the idea that thalamic connections to cortex are differentially affected by propofol. Experimental and modeling work have previously demonstrated that the alpha rhythms in sensory thalamocortical circuits are altered in a distinct manner from higher order thalamocortical circuits (Soplata et al., 2023; Weiner et al., 2023; Flores et al., 2017; Vijayan et al., 2013). As a consequence, thalamic relay to sensory cortex may continue (albeit with altered dynamics), but long-range communication of sensory information may be impaired by the differential effect of propofol on higher order thalamocortical circuits (Liu et al., 2013). Interestingly, electrical stimulation of the thalamus increases arousal and has been shown to restore aspects of consciousness (Tasserie et al., 2022; Afrasiabi et al., 2021; Bastos et al., 2021; Redinbaugh et al., 2020). Whether it can fully restore sensory processing will be addressed in future work.

Our results are also in line with theories suggesting anesthesia primarily disrupts sensory processing within cortex. One such theory proposes a "multiple hit mechanism." Many small perturbations add up along sensory processing pathways (Krom et al., 2020). Our results instead suggest a large drop-off between sensory cortex and parietal/frontal cortex. However, we did not record from all of cortex so we may have not observed other perturbations. Our findings also align with Dehaene and Changeux (2011). They hypothesize conscious awareness relies on broadcasting cortical activity across cortex through long-range projections. A disruption of long-range cortical communication would presumably also disrupt the integration of information that the integrated information theory suggests is necessary for the conscious state (Tononi, Boly, Massimini, & Koch, 2016).

As a limitation of our study, we focused specifically on propofol's impact on sensory processing and did not analyze the conditioning component of the auditory stimuli. Thus, we do not draw any conclusions about differences in the conditioned and unconditioned tone, but we suggest this is an interesting avenue for future research. We also did not directly investigate sleep or other anesthetics in this study. Although we draw connections to sleep and other anesthetics above, further studies will be needed to clarify the similarities and differences across these various altered states of consciousness.

In summary, we have shown propofol anesthesia eliminates stimulus-related alpha–beta synchronization between cortical areas and progressively disrupts information processing along the cortical hierarchy. These neural signatures of propofol-mediated unconsciousness may be fruitful targets for monitoring to avoid intraoperative awareness.

APPENDIX A: ADDITIONAL SYNCHRONY MEASURES

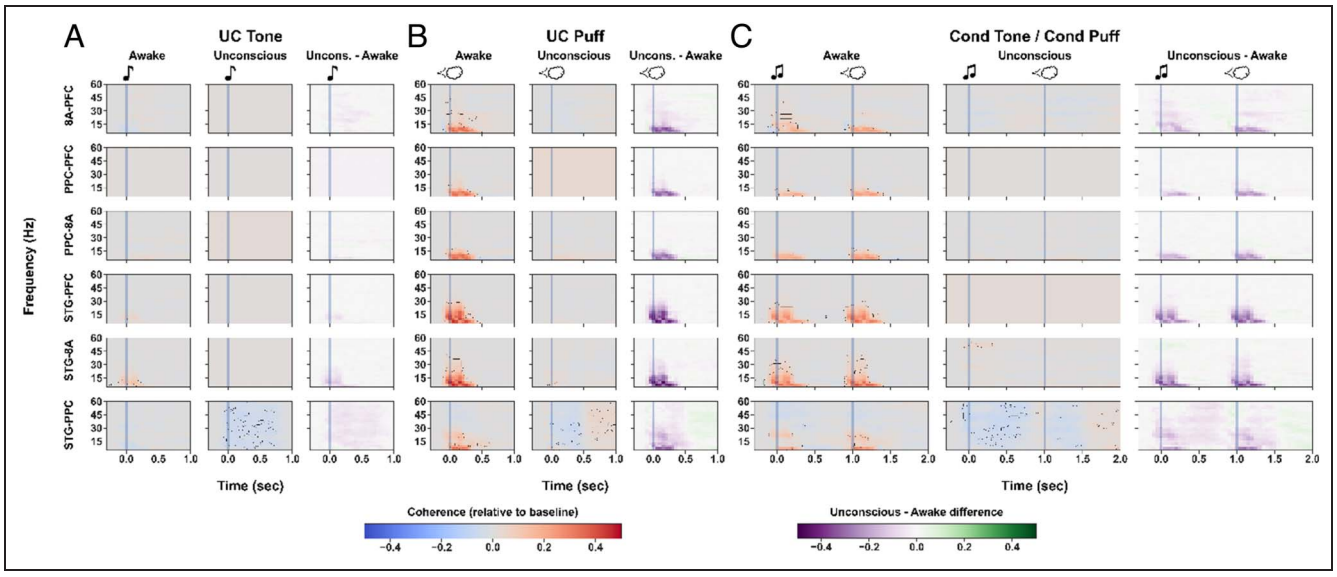

Figure A1. Total PLV quantification of stimulus-related synchronization. Plots show the same analysis as in Figure 5, but without removal of the trial-averaged response from the time-domain. (A–C) Stimulus-related change from baseline synchrony in Awake (left) and Unconscious (middle) for indicated stimuli. The right column shows the difference between Unconscious and Awake. Contour lines show regions of statistical significance (Wilcoxon).

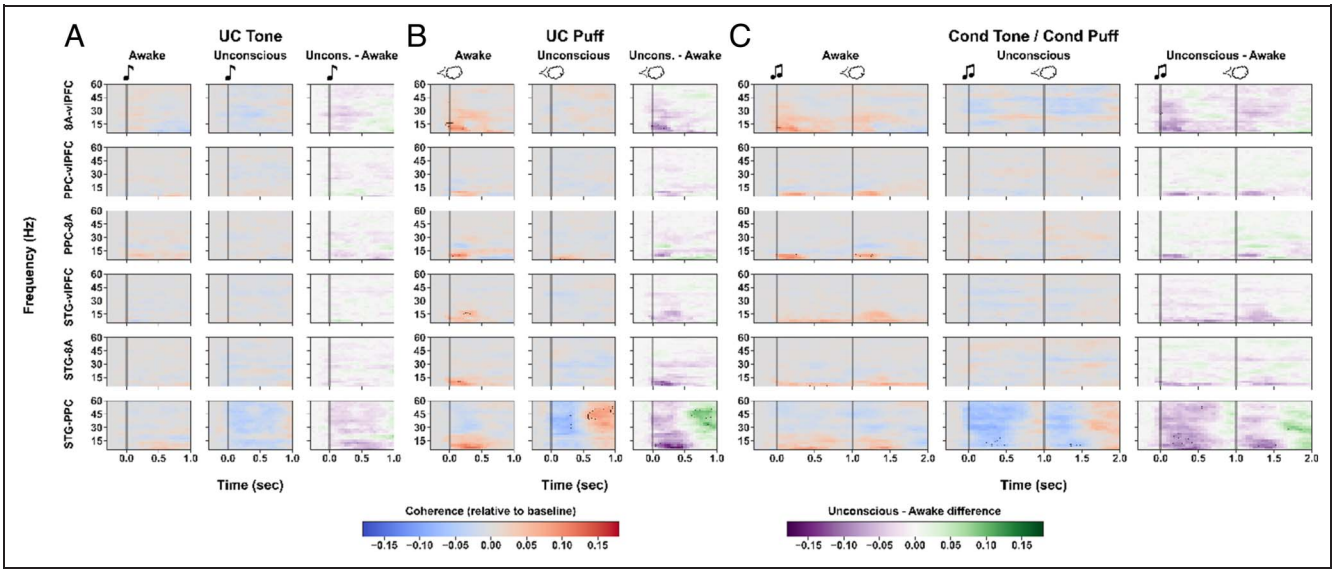

Figure A2. Induced coherence quantification of stimulus-related synchronization. Plots show the same analysis as in Figure 5 but use coherence to measure synchronization instead of a PLV (see Methods section). (A–C) Stimulus-related change from baseline synchrony in Awake (left) and Unconscious (middle) for indicated stimuli. The right column shows the difference between Unconscious and Awake. Contour lines show regions of statistical significance (t test on z-transformed of values; see Methods).

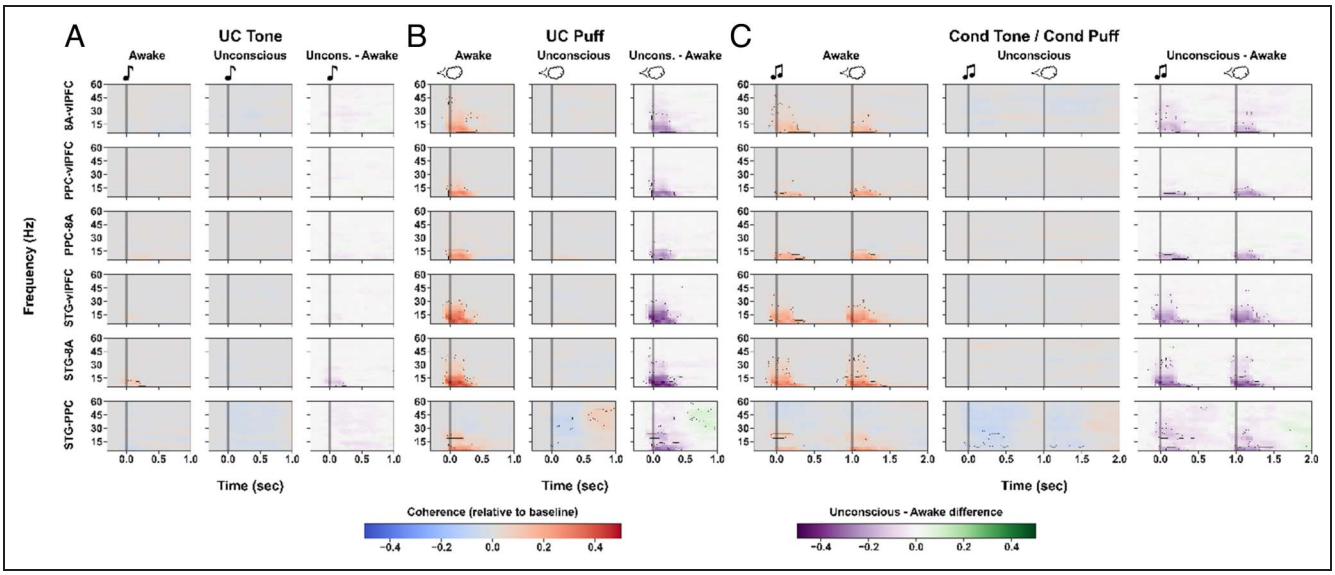

Figure A3. Total coherence quantification of stimulus-related synchronization. Plots show the same analysis as in Figure A1 (i.e., trial-averaged response is not subtracted in the time-domain) but use coherence to measure synchronization instead of a PLV. (A–C) Stimulus-related change from baseline synchrony in Awake (left) and Unconscious (middle) for indicated stimuli. The right column shows the difference between Unconscious and Awake. Contour lines show regions of statistical significance (t test on z-transformed of values; see Methods).

APPENDIX B: ADDITIONAL TECHNICAL DETAILS FOR HMM

To simplify notation moving forward, we vectorize the history term component of the CIF as

$$\boldsymbol{\alpha}^{\top}\boldsymbol{h}_t^c = \sum_{\ell=1}^{L} \alpha_\ell n_{t-\ell}^c \tag{B1}$$

where $\boldsymbol{\alpha} = (\alpha_1, \ldots, \alpha_L)^{\top}$ and $\boldsymbol{h}_t^c = \left(n_{t-1}^c, \ldots, n_{t-L}\right)^{\top}$. The stimulus terms component is vectorized as

$$\boldsymbol{\beta}^{\top}\boldsymbol{u}_t = \sum_{s=1}^{S}\sum_{j=1}^{J} \beta_j^{k^*,s} B_{t,j}^{k^*,s} \tag{B2}$$

where, using $\boldsymbol{\beta}^{k^*,s} = \left(\beta_1^{k^*,s}, \ldots, \beta_J^{k^*,s}\right)$ and $\boldsymbol{B}_t^{k^*,s} = \left(B_{t,1}^{k^*,s}, \ldots, B_{t,J}^{k^*,s}\right)$ we have concatenated:

$$\boldsymbol{\beta} = \begin{bmatrix} \boldsymbol{\beta}^{0,0}, \boldsymbol{\beta}^{1,0}, \ldots, \boldsymbol{\beta}^{K^*,0}, \boldsymbol{\beta}^{0,1}, \boldsymbol{\beta}^{1,1}, \ldots, \boldsymbol{\beta}^{K^*,1}, \ldots\ldots, \boldsymbol{\beta}^{0,S}, \\ \boldsymbol{\beta}^{1,S}, \ldots, \boldsymbol{\beta}^{K^*,S} \end{bmatrix}^{\top}$$

$$\boldsymbol{u}_t = \begin{bmatrix} \boldsymbol{B}_t^{0,0}, \boldsymbol{B}_t^{1,0}, \ldots, \boldsymbol{B}_t^{K^*,0}, \boldsymbol{B}_t^{0,1}, \boldsymbol{B}_t^{1,1}, \ldots, \boldsymbol{B}_t^{K^*,1}, \ldots\ldots, \boldsymbol{B}_t^{0,S}, \\ \boldsymbol{B}_t^{1,S}, \ldots, \boldsymbol{B}_t^{K^*,S} \end{bmatrix}^{\top}$$

Using this simplified notation, the CIF can now be written:

$$\log \lambda_t^{k,c} = \mu^{k,c} + \boldsymbol{\alpha}^{\top}\boldsymbol{h}_t^c + \boldsymbol{\beta}^{\top}\boldsymbol{u}_t \tag{B3}$$

EM Algorithm

Letting $\boldsymbol{n}_t = \left(n_t^1, \ldots, n_t^C\right)^{\top}$, we assume that the neurons are conditionally independent given the hidden state and spiking history and write the joint probability as:

$$\begin{aligned} &P(\boldsymbol{z}_{1:T}, \boldsymbol{n}_{1:T}|\boldsymbol{\theta}) \\ &\quad = P(\boldsymbol{z}_1|\boldsymbol{\theta}) \prod_{t=2}^{T} P(\boldsymbol{z}_t|\boldsymbol{z}_{t-1}, \boldsymbol{\theta}) \prod_{t=1}^{T}\prod_{c=1}^{C} P\left(n_t^c|\boldsymbol{z}_t, \boldsymbol{H}_t^c, \boldsymbol{\theta}\right) \end{aligned} \tag{B4}$$

In the EM algorithm, our goal is to maximize the complete-data log likelihood:

$$\begin{aligned} \log \mathcal{L}(\boldsymbol{\theta}) = &\log P(\boldsymbol{z}_1|\boldsymbol{\theta}) + \sum_{t=2}^{T} \log P(\boldsymbol{z}_t|\boldsymbol{z}_{t-1}, \boldsymbol{\theta}) \\ &+ \sum_{t=1}^{T}\sum_{c=1}^{C} \log P\left(n_t^c|\boldsymbol{z}_t, \boldsymbol{H}_t^c, \boldsymbol{\theta}\right) \end{aligned} \tag{B5}$$

which under our observation model can be written:

$$\begin{aligned} \log \mathcal{L}(\boldsymbol{\theta}) = &\sum_{k=1}^{K} z_1^k \log \pi^k + \sum_{t=2}^{T}\sum_{j=1}^{K}\sum_{k=1}^{K} z_t^k z_{t-1}^j \log A_{j,k} \\ &+ \sum_{t=1}^{T}\sum_{c=1}^{C}\sum_{k=1}^{K} z_t^k \left[n_t^c \log\left(\lambda_t^{k,c}\Delta\right) - \lambda_t^{k,c}\Delta\right] \end{aligned} \tag{B6}$$

Details on the form of the point process component of Equation B6 can be found in Smith and Brown (2003). We define the Q-function as the expectation of the complete data log likelihood, on iteration $r + 1$ of the EM algorithm, using the parameters $\boldsymbol{\theta}^{(r)}$ from the previous iteration:

$$\begin{aligned} Q\left(\boldsymbol{\theta}|\boldsymbol{\theta}^{(r)}\right) &= \mathrm{E}_{\boldsymbol{z}_{1:T}|\boldsymbol{n}_{1:T}}\left[\log \mathcal{L}(\boldsymbol{\theta})|\boldsymbol{n}_{1:T}, \boldsymbol{\theta}^{(r)}\right] \\ &= \sum_{z} P\left(\boldsymbol{z}_{1:T}|\boldsymbol{n}_{1:T}, \boldsymbol{\theta}^{(r)}\right) \log P(\boldsymbol{z}_{1:T}, \boldsymbol{n}_{1:T}|\boldsymbol{\theta}) \end{aligned} \tag{B7}$$

and following Bishop (2006), we introduce the following notation:

$$\gamma\left(z_t^k\right) = \mathrm{E}\left[z_t^k|\boldsymbol{n}_{1:T}, \boldsymbol{\theta}^{(r)}\right]$$

$$\xi\left(z_{t-1}^j, z_t^k\right) = \mathrm{E}\left[z_{t-1}^j, z_t^k|\boldsymbol{n}_{1:T}, \boldsymbol{\theta}^{(r)}\right]$$

where the expectation is taken over the conditional distribution of the hidden states given the data. We can now write the full Q-function:

$$\begin{aligned} Q\left(\boldsymbol{\theta}|\boldsymbol{\theta}^{(r)}\right) = &\sum_{k=1}^{K} \gamma\left(z_1^k\right) \log \pi^k + \sum_{t=1}^{T}\sum_{j=1}^{K}\sum_{k=1}^{K} \xi\left(z_{t-1}^j, z_t^k\right) \log A_{j,k} \\ &+ \sum_{t=1}^{T}\sum_{c=1}^{C}\sum_{k=1}^{K} \gamma\left(z_t^k\right)\left[n_t^c\left(\log\Delta + \mu^{k,c} + \boldsymbol{\alpha}^{\top}\boldsymbol{h}_t^c + \boldsymbol{\beta}^{\top}\boldsymbol{u}_t\right)\right. \\ &\left. - \exp\left(\mu^{k,c} + \boldsymbol{\alpha}^{\top}\boldsymbol{h}_t^c + \boldsymbol{\beta}^{\top}\boldsymbol{u}_t\right)\Delta\right] \end{aligned}$$

The closed form estimates for $\boldsymbol{\pi}$ and $\mathbf{A}$ are:

$$\begin{aligned} \pi^k &= \frac{\gamma\left(z_1^k\right)}{\sum_{j=1}^{K} \gamma\left(z_1^k\right)} \\ A_{j,k} &= \frac{\sum_{t=1}^{T} \xi\left(z_{t-1}^j, z_t^k\right)}{\sum_{k=1}^{K}\sum_{t=1}^{T} \xi\left(z_{t-1}^j, z_t^k\right)} \end{aligned} \tag{B8}$$

In the Broyden-Fletcher-Goldfarb-Shanno algorithm used to numerically estimate the point-process parameters, we use the following gradients:

$$\begin{aligned} \frac{\partial Q\left(\boldsymbol{\theta}|\boldsymbol{\theta}^{(r)}\right)}{\partial \mu^{k,c}} &= \sum_{t=1}^{T} \gamma\left(z_t^k\right)\left[n_t^c - \exp\left(\mu^{k,c} + \boldsymbol{\alpha}^{\top}\boldsymbol{h}_t^c + \boldsymbol{\beta}^{\top}\boldsymbol{u}_t\right)\Delta\right] \\ \frac{\partial Q\left(\boldsymbol{\theta}|\boldsymbol{\theta}^{(r)}\right)}{\partial \boldsymbol{\alpha}} &= \sum_{t=1}^{T}\sum_{k=1}^{K}\sum_{c=1}^{C} \gamma\left(z_t^k\right) \\ &\quad \left[n_t^c \boldsymbol{h}_t^c - \boldsymbol{h}_t^c \exp\left(\mu^{k,c} + \boldsymbol{\alpha}^{\top}\boldsymbol{h}_t^c + \boldsymbol{\beta}^{\top}\boldsymbol{u}_t\right)\Delta\right] \\ \frac{\partial Q\left(\boldsymbol{\theta}|\boldsymbol{\theta}^{(r)}\right)}{\partial \boldsymbol{\beta}} &= \sum_{t=1}^{T}\sum_{k=1}^{K}\sum_{c=1}^{C} \gamma\left(z_t^k\right) \\ &\quad \left[n_t^c \boldsymbol{u}_t - \boldsymbol{u}_t \exp\left(\mu^{k,c} + \boldsymbol{\alpha}^{\top}\boldsymbol{h}_t^c + \boldsymbol{\beta}^{\top}\boldsymbol{u}_t\right)\Delta\right] \end{aligned} \tag{B9}$$

Louis Method for Confidence Intervals

Louis (1982) developed a method that enables calculating the observed Fisher information when using the EM

algorithm (Efron & Hinkley, 1978). We use this method for calculating confidence intervals on the estimated spiking response. The method calculates the "observed information" $\boldsymbol{I_n}$ as:

$$\boldsymbol{I_n} = \boldsymbol{I_{zn}} - \boldsymbol{I_{z|n}} \tag{B10}$$

where $\boldsymbol{I_{z|n}}$ is the "complete information" calculated from the Hessian of the Q-function, and $\boldsymbol{I_{z|n}}$ is the "missing information," which provides a correction term to account for the fact that we lose information by taking the expected value of the hidden variables.

$$\boldsymbol{I_{zn}} = -\frac{\partial^2 Q\left(\boldsymbol{\theta}|\hat{\boldsymbol{\theta}}\right)}{\partial \boldsymbol{\theta} \partial \boldsymbol{\theta}^\top}\bigg|_{\boldsymbol{\theta}=\hat{\boldsymbol{\theta}}} \tag{B11}$$

$$\boldsymbol{I_{z|n}} = \mathrm{E}_{\boldsymbol{z}|\boldsymbol{n}}\left[S(\boldsymbol{z}, \boldsymbol{n}|\boldsymbol{\theta}) S(\boldsymbol{z}, \boldsymbol{n}|\boldsymbol{\theta})^\top\right] \tag{B12}$$

where

$$S(\boldsymbol{z}, \boldsymbol{n}|\boldsymbol{\theta}) = \frac{\partial Q\left(\boldsymbol{\theta}|\hat{\boldsymbol{\theta}}\right)}{\partial \boldsymbol{\theta}}$$

We calculated $\boldsymbol{I_{z|n}}$ using a Monte Carlo approximation as in Turner, Cameron, and Thomson (1998):

$$\mathrm{E}_{\boldsymbol{z}|\boldsymbol{n}}\left[S(\boldsymbol{z}, \boldsymbol{n}|\boldsymbol{\theta}) S(\boldsymbol{z}, \boldsymbol{n}|\boldsymbol{\theta})^\top\right] \approx \frac{1}{M}\sum_{m=1}^{M} S\left(\boldsymbol{z}^{(m)}, \boldsymbol{n}|\boldsymbol{\theta}\right) S\left(\boldsymbol{z}^{(m)}, \boldsymbol{n}|\boldsymbol{\theta}\right)^\top \tag{B13}$$

where the $\boldsymbol{z}^{(m)}$ are sampled from the posterior distribution of the hidden states given the data. We used $M = 50$ Monte Carlo samples for all sessions. The Hessian of the Q-function can be computed using the following:

$$\begin{aligned}
\frac{\partial^2 Q\left(\boldsymbol{\theta}|\boldsymbol{\theta}^{(r)}\right)}{\partial\left(\mu^{k,c}\right)^2} &= \sum_{t=1}^{T}\sum_{k=1}^{K} \gamma\left(z_t^k\right)\left[-\exp\left(\mu^{k,c} + \boldsymbol{\alpha}^\top \boldsymbol{b}_t^c + \boldsymbol{\beta}^\top \boldsymbol{u}_t\right)\Delta\right] \\
\frac{\partial^2 Q\left(\boldsymbol{\theta}|\boldsymbol{\theta}^{(r)}\right)}{\partial \boldsymbol{\alpha} \partial \boldsymbol{\alpha}^\top} &= \sum_{t=1}^{T}\sum_{k=1}^{K}\sum_{c=1}^{C} \gamma\left(z_t^k\right) \\
&\quad \left[-\boldsymbol{b}_t^c \boldsymbol{b}_t^{c^\top} \exp\left(\mu^{k,c} + \boldsymbol{\alpha}^\top \boldsymbol{b}_t^c + \boldsymbol{\beta}^\top \boldsymbol{u}_t\right)\Delta\right] \\
\frac{\partial^2 Q\left(\boldsymbol{\theta}|\boldsymbol{\theta}^{(r)}\right)}{\partial \boldsymbol{\beta} \partial \boldsymbol{\beta}^\top} &= \sum_{t=1}^{T}\sum_{k=1}^{K}\sum_{c=1}^{C} \gamma\left(z_t^k\right) \\
&\quad \left[-\boldsymbol{u}_t \boldsymbol{u}_t^\top \exp\left(\mu^{k,c} + \boldsymbol{\alpha}^\top \boldsymbol{b}_t^c + \boldsymbol{\beta}^\top \boldsymbol{u}_t\right)\Delta\right]
\end{aligned} \tag{B14}$$

Acknowledgments

We thank Andre Bastos, Josefina Correa, Uri Eden, Adam Eisen, and Indie Garwood for helpful comments and feedback.

Corresponding author: Earl K. Miller, Department of Brain and Cognitive Sciences, Massachusetts Institute of Technology, 77 Massachusetts Ave., Cambridge, MA 02139, USA, or via e-mail: ekmiller@mit.edu.

Data Availability Statement

Code used for analysis can be found at github.com/johntauber/propofol_sensory. The data will be made available by reasonable request by contacting the corresponding author.

Author Contributions

John Tauber: Formal analysis; Methodology; Writing—Original draft; Writing—Review & editing. Scott L. Brincat: Data curation; Investigation; Methodology; Writing—Review & editing. Emily P. Stephen: Methodology; Writing—Review & editing. Jacob A. Donoghue: Investigation. Leo Kozachkov: Software; Writing—Review & editing. Emery N. Brown: Conceptualization; Funding acquisition; Project administration; Supervision; Writing—Review & editing. Earl K. Miller: Conceptualization; Funding acquisition; Project administration; Supervision; Writing—Original draft; Writing—Review & editing.

Funding Information

This study was supported by Office of Naval Research N000142212453, NINDS R01NS123120, NIMH R01MH11559, NIGMS P01GM118269, The Picower Institute for Learning and Memory, and The JPB Foundation.

Diversity in Citation Practices

Retrospective analysis of the citations in every article published in this journal from 2010 to 2021 reveals a persistent pattern of gender imbalance: Although the proportions of authorship teams (categorized by estimated gender identification of first author/last author) publishing in the *Journal of Cognitive Neuroscience* (*JoCN*) during this period were M(an)/M = .407, W(oman)/M = .32, M/W = .115, and W/W = .159, the comparable proportions for the articles that these authorship teams cited were M/M = .549, W/M = .257, M/W = .109, and W/W = .085 (Postle and Fulvio, *JoCN*, 34:1, pp. 1–3). Consequently, *JoCN* encourages all authors to consider gender balance explicitly when selecting which articles to cite and gives them the opportunity to report their article's gender citation balance.

REFERENCES

Afrasiabi, M., Redinbaugh, M. J., Phillips, J. M., Kambi, N. A., Mohanta, S., Raz, A., et al. (2021). Consciousness depends on integration between parietal cortex, striatum, and thalamus. *Cell Systems*, *12*, 363–373. https://doi.org/10.1016/j.cels.2021.02.003, PubMed: 33730543

Akeju, O., & Brown, E. N. (2017). Neural oscillations demonstrate that general anesthesia and sedative states are neurophysiologically distinct from sleep. *Current Opinion in Neurobiology*, *44*, 178–185. https://doi.org/10.1016/j.conb.2017.04.011, PubMed: 28544930

Alenda, A., Molano-Mazón, M., Panzeri, S., & Maravall, M. (2010). Sensory input drives multiple intracellular

information streams in somatosensory cortex. *Journal of Neuroscience*, *30*, 10872–10884. https://doi.org/10.1523/JNEUROSCI.6174-09.2010, PubMed: 20702716

Alkire, M. T., Haier, R. J., & Fallon, J. H. (2000). Toward a unified theory of narcosis: Brain imaging evidence for a thalamocortical switch as the neurophysiologic basis of anesthetic-induced unconsciousness. *Consciousness and Cognition*, *9*, 370–386. https://doi.org/10.1006/ccog.1999.0423, PubMed: 10993665

Andrillon, T., & Kouider, S. (2020). The vigilant sleeper: Neural mechanisms of sensory (de)coupling during sleep. *Current Opinion in Physiology*, *15*, 47–59. https://doi.org/10.1016/j.cophys.2019.12.002

Andrillon, T., Poulsen, A. T., Hansen, L. K., Léger, D., & Kouider, S. (2016). Neural markers of responsiveness to the environment in human sleep. *Journal of Neuroscience*, *36*, 6583–6596. https://doi.org/10.1523/JNEUROSCI.0902-16.2016, PubMed: 27307244

Arieli, A., Sterkin, A., Grinvald, A., & Aertsen, A. (1996). Dynamics of ongoing activity: Explanation of the large variability in evoked cortical responses. *Science*, *273*, 1868–1871. https://doi.org/10.1126/science.273.5283.1868, PubMed: 8791593

Azouz, R., & Gray, C. M. (1999). Cellular mechanisms contributing to response variability of cortical neurons in vivo. *Journal of Neuroscience*, *19*, 2209–2223. https://doi.org/10.1523/JNEUROSCI.19-06-02209.1999, PubMed: 10066274

Babadi, B., & Brown, E. N. (2014). A review of multitaper spectral analysis. *IEEE Transactions on Biomedical Engineering*, *61*, 1555–1564. https://doi.org/10.1109/TBME.2014.2311996, PubMed: 24759284

Bai, D., Pennefather, P. S., MacDonald, J. F., & Orser, B. A. (1999). The general anesthetic propofol slows deactivation and desensitization of GABA(a) receptors. *Journal of Neuroscience*, *19*, 10635–10646. https://doi.org/10.1523/JNEUROSCI.19-24-10635.1999, PubMed: 10594047

Banks, M. I., Krause, B. M., Endemann, C. M., Campbell, D. I., Kovach, C. K., Dyken, M. E., et al. (2020). Cortical functional connectivity indexes arousal state during sleep and anesthesia. *Neuroimage*, *211*, 116627. https://doi.org/10.1016/j.neuroimage.2020.116627, PubMed: 32045640

Banks, M., Moran, N., Krause, B., Grady, S., Uhlrich, D., & Manning, K. (2018). Altered stimulus representation in rat auditory cortex is not causal for loss of consciousness under general anaesthesia. *British Journal of Anaesthesia*, *121*, 605–615. https://doi.org/10.1016/j.bja.2018.05.054, PubMed: 30115259

Bartels, R. H., Beatty, J. C., & Barsky, B. A. (1995). *An introduction to splines for use in computer graphics and geometric modeling*. Morgan Kaufmann.

Bastos, A. M., Donoghue, J. A., Brincat, S. L., Mahnke, M., Yanar, J., Correa, J., et al. (2021). Neural effects of propofol-induced unconsciousness and its reversal using thalamic stimulation. *eLife*, *10*, e60284. https://doi.org/10.7554/eLife.60824, PubMed: 33904411

Bastos, A. M., Vezoli, J., Bosman, C. A., Schoffelen, J.-M., Oostenveld, R., Dowdall, J. R., et al. (2015). Visual areas exert feedforward and feedback influences through distinct frequency channels. *Neuron*, *85*, 390–401. https://doi.org/10.1016/j.neuron.2014.12.018, PubMed: 25556836

Bishop, C. M. (2006). *Pattern recognition and machine learning* (*Vol. 4*). Springer. https://www.microsoft.com/en-us/research/uploads/prod/2006/01/Bishop-Pattern-Recognition-and-Machine-Learning-2006.pdf

Boly, M., Moran, R., Murphy, M., Boveroux, P., Bruno, M.-A., Noirhomme, Q., et al. (2012). Connectivity changes underlying spectral EEG changes during propofol-induced loss of consciousness. *Journal of Neuroscience*, *32*, 7082–7090. https://doi.org/10.1523/JNEUROSCI.3769-11.2012, PubMed: 22593076

Boveroux, P., Vanhaudenhuyse, A., Bruno, M. A., Noirhomme, Q., Lauwick, S., Luxen, A., et al. (2010). Breakdown of within- and between-network resting state functional magnetic resonance imaging connectivity during propofol-induced loss of consciousness. *Anesthesiology*, *113*, 1038–1053. https://doi.org/10.1097/ALN.0b013e3181f697f5, PubMed: 20885292

Brincat, S. L. (2023). *spynal: Simple Python Neural Analysis Library (v0.1.2)* [Computer software]. https://doi.org/10.5281/zenodo.8346152

Brown, E. N., Lydic, R., & Schiff, N. D. (2010). General anesthesia, sleep, and coma. *New England Journal of Medicine*, *363*, 2638–2650. https://doi.org/10.1056/NEJMra0808281, PubMed: 21190458

Brown, E. N., Purdon, P. L., & Van Dort, C. J. (2011). General anesthesia and altered states of arousal: A systems neuroscience analysis. *Annual Review of Neuroscience*, *34*, 601–628. https://doi.org/10.1146/annurev-neuro-060909-153200, PubMed: 21513454

Buzsáki, G., Anastassiou, C. A., & Koch, C. (2012). The origin of extracellular fields and currents—EEG, ECoG, LFP and spikes. *Nature Reviews Neuroscience*, *13*, 407–420. https://doi.org/10.1038/nrn3241, PubMed: 22595786

Cajigas, I., Davis, K. C., Meschede-Krasa, B., Prins, N. W., Gallo, S., Naeem, J. A., et al. (2021). Implantable brain–computer interface for neuroprosthetic-enabled volitional hand grasp restoration in spinal cord injury. *Brain Communications*, *3*, fcab248. https://doi.org/10.1093/braincomms/fcab248, PubMed: 34870202

Camassa, A., Galluzzi, A., Mattia, M., & Sanchez-Vives, M. V. (2022). Deterministic and stochastic components of cortical down states: Dynamics and modulation. *Journal of Neuroscience*, *42*, 9387–9400. https://doi.org/10.1523/JNEUROSCI.0914-22.2022, PubMed: 36344267

Chen, Z., Vijayan, S., Barbieri, R., Wilson, M. A., & Brown, E. N. (2009). Discrete-and continuous-time probabilistic models and algorithms for inferring neuronal UP and DOWN states. *Neural Computation*, *21*, 1797–1862. https://doi.org/10.1162/neco.2009.06-08-799, PubMed: 19323637

Ching, S., Cimenser, A., Purdon, P. L., Brown, E. N., & Kopell, N. J. (2010). Thalamocortical model for a propofol-induced alpha-rhythm associated with loss of consciousness. *Proceedings of the National Academy of Sciences, U.S.A.*, *107*, 22665–22670. https://doi.org/10.1073/pnas.1017069108, PubMed: 21149695

Cohen, M. X. (2014). *Analyzing neural time series data: Theory and practice*. MIT Press. https://mikexcohen.com/book/Cohen_AnalyzingNeuralTimeSeriesData_TOC.pdf. https://doi.org/10.7551/mitpress/9609.001.0001

Cortes, C., & Vapnik, V. (1995). Support-vector networks. *Machine Learning*, *20*, 273–297. https://doi.org/10.1007/BF00994018

Cosgrove, M. E., Saadon, J. R., Mikell, C. B., Stefancin, P. L., Alkadaa, L., Wang, Z., et al. (2022). Thalamo-prefrontal connectivity correlates with early command-following after severe traumatic brain injury. *Frontiers in Neurology*, *13*, 826266. https://doi.org/10.3389/fneur.2022.826266, PubMed: 35250829

Cramér, H. (1999). *Mathematical methods of statistics* (Vol. 26). Princeton University Press. https://doi.org/10.1515/9781400883868

Crowe, D. A., Goodwin, S. J., Blackman, R. K., Sakellaridi, S., Sponheim, S. R., MacDonald, A. W., III, et al. (2013). Prefrontal neurons transmit signals to parietal neurons that reflect executive control of cognition. *Nature Neuroscience*, *16*, 1484–1491. https://doi.org/10.1038/nn.3509, PubMed: 23995071

Daley, D. J., & Vere-Jones, D. (2003). *An introduction to the theory of point processes: Volume I: Elementary theory and methods*. Springer. https://doi.org/10.1007/b97277
David, O., Kilner, J. M., & Friston, K. J. (2006). Mechanisms of evoked and induced responses in MEG/EEG. *Neuroimage*, *31*, 1580–1591. https://doi.org/10.1016/j.neuroimage.2006.02.034, PubMed: 16632378
Davis, M. H., Coleman, M. R., Absalom, A. R., Rodd, J. M., Johnsrude, I. S., Matta, B. F., et al. (2007). Dissociating speech perception and comprehension at reduced levels of awareness. *Proceedings of the National Academy of Sciences, U.S.A.*, *104*, 16032–16037. https://doi.org/10.1073/pnas.0701309104, PubMed: 17938125
Dehaene, S., & Changeux, J.-P. (2011). Experimental and theoretical approaches to conscious processing. *Neuron*, *70*, 200–227. https://doi.org/10.1016/j.neuron.2011.03.018, PubMed: 21521609
Dempster, A. P., Laird, N. M., & Rubin, D. B. (1977). Maximum likelihood from incomplete data via the EM algorithm. *Journal of the Royal Statistical Society: Series B (Methodological)*, *39*, 1–38. https://doi.org/10.1111/j.2517-6161.1977.tb01600.x
Destexhe, A., Hughes, S. W., Rudolph, M., & Crunelli, V. (2007). Are corticothalamic 'up' states fragments of wakefulness? *Trends in Neurosciences*, *30*, 334–342. https://doi.org/10.1016/j.tins.2007.04.006, PubMed: 17481741
Doob, J. L. (1935). The limiting distributions of certain statistics. *Annals of Mathematical Statistics*, *6*, 160–169. https://doi.org/10.1214/aoms/1177732594
Efron, B., & Hinkley, D. V. (1978). Assessing the accuracy of the maximum likelihood estimator: Observed versus expected fisher information. *Biometrika*, *65*, 457–483. https://doi.org/10.1093/biomet/65.3.457
Filipchuk, A., Schwenkgrub, J., Destexhe, A., & Bathellier, B. (2022). Awake perception is associated with dedicated neuronal assemblies in the cerebral cortex. *Nature Neuroscience*, *25*, 1327–1338. https://doi.org/10.1038/s41593-022-01168-5, PubMed: 36171431
Fletcher, R. (2013). *Practical methods of optimization*. John Wiley & Sons. https://doi.org/10.1002/9781118723203
Flores, F. J., Hartnack, K. E., Fath, A. B., Kim, S. E., Wilson, M. A., Brown, E. N., et al. (2017). Thalamocortical synchronization during induction and emergence from propofol-induced unconsciousness. *Proceedings of the National Academy of Sciences, U.S.A.*, *114*, E6660–E6668. https://doi.org/10.1073/pnas.1700148114, PubMed: 28743752
Fries, P. (2005). A mechanism for cognitive dynamics: Neuronal communication through neuronal coherence. *Trends in Cognitive Sciences*, *9*, 474–480. https://doi.org/10.1016/j.tics.2005.08.011, PubMed: 16150631
Fries, P. (2015). Rhythms for cognition: Communication through coherence. *Neuron*, *88*, 220–235. https://doi.org/10.1016/j.neuron.2015.09.034, PubMed: 26447583
Fries, P., & Maris, E. (2022). What to do if N is two? *Journal of Cognitive Neuroscience*, *34*, 1114–1118. https://doi.org/10.1162/jocn_a_01857, PubMed: 35468209
Garwood, I. C., Chakravarty, S., Donoghue, J., Mahnke, M., Kahali, P., Chamadia, S., et al. (2021). A Hidden Markov Model reliably characterizes ketamine-induced spectral dynamics in macaque local field potentials and human electroencephalograms. *PLoS Computational Biology*, *17*, e1009280. https://doi.org/10.1371/journal.pcbi.1009280, PubMed: 34407069
Ghoneim, M. M. (2000). Awareness during anesthesia. *Anesthesiology*, *92*, 597–602. https://doi.org/10.1097/00000542-200002000-00043, PubMed: 10691248
Haider, B., Duque, A., Hasenstaub, A. R., Yu, Y., & McCormick, D. A. (2007). Enhancement of visual responsiveness by spontaneous local network activity in vivo. *Journal of Neurophysiology*, *97*, 4186–4202. https://doi.org/10.1152/jn.01114.2006, PubMed: 17409168
Hamilton, J. D. (1990). Analysis of time series subject to changes in regime. *Journal of Econometrics*, *45*, 39–70. https://doi.org/10.1016/0304-4076(90)90093-9
Hasenstaub, A., Sachdev, R. N., & McCormick, D. A. (2007). State changes rapidly modulate cortical neuronal responsiveness. *Journal of Neuroscience*, *27*, 9607–9622. https://doi.org/10.1523/JNEUROSCI.2184-07.2007, PubMed: 17804621
Hastie, T., Tibshirani, R., & Friedman, J. H. (2009). *The elements of statistical learning: Data mining, inference, and prediction* (Vol. 2). Springer. https://hastie.su.domains/ElemStatLearn/. https://doi.org/10.1007/978-0-387-84858-7
Hayat, H., Marmelshtein, A., Krom, A. J., Sela, Y., Tankus, A., Strauss, I., et al. (2022). Reduced neural feedback signaling despite robust neuron and gamma auditory responses during human sleep. *Nature Neuroscience*, *25*, 935–943. https://doi.org/10.1038/s41593-022-01107-4, PubMed: 35817847
Heinke, W., Kenntner, R., Gunter, T. C., Sammler, D., Olthoff, D., & Koelsch, S. (2004). Sequential effects of increasing propofol sedation on frontal and temporal cortices as indexed by auditory event-related potentials. *Anesthesiology*, *100*, 617–625. https://doi.org/10.1097/00000542-200403000-00023, PubMed: 15108977
Hemmings, H. C., Akabas, M. H., Goldstein, P. A., Trudell, J. R., Orser, B. A., & Harrison, N. L. (2005). Emerging molecular mechanisms of general anesthetic action. *Trends in Pharmacological Sciences*, *26*, 503–510. https://doi.org/10.1016/j.tips.2005.08.006, PubMed: 16126282
Hemmings, H. C., Riegelhaupt, P. M., Kelz, M. B., Solt, K., Eckenhoff, R. G., Orser, B. A., et al. (2019). Towards a comprehensive understanding of anesthetic mechanisms of action: A decade of discovery. *Trends in Pharmacological Sciences*, *40*, 464–481. https://doi.org/10.1016/j.tips.2019.05.001, PubMed: 31147199
Hoffman, K. L., Battaglia, F. P., Harris, K., MacLean, J. N., Marshall, L., & Mehta, M. R. (2007). The upshot of up states in the neocortex: From slow oscillations to memory formation. *Journal of Neuroscience*, *27*, 11838–11841. https://doi.org/10.1523/JNEUROSCI.3501-07.2007, PubMed: 17978020
Imas, O. A., Ropella, K. M., Ward, B. D., Wood, J. D., & Hudetz, A. G. (2005). Volatile anesthetics disrupt frontal-posterior recurrent information transfer at gamma frequencies in rat. *Neuroscience Letters*, *387*, 145–150. https://doi.org/10.1016/j.neulet.2005.06.018, PubMed: 16019145
Ishizawa, Y., Ahmed, O. J., Patel, S. R., Gale, J. T., Sierra-Mercado, D., Brown, E. N., et al. (2016). Dynamics of propofol-induced loss of consciousness across primate neocortex. *Journal of Neuroscience*, *36*, 7718–7726. https://doi.org/10.1523/JNEUROSCI.4577-15.2016, PubMed: 27445148
Issa, E. B., & Wang, X. (2011). Altered neural responses to sounds in primate primary auditory cortex during slow-wave sleep. *Journal of Neuroscience*, *31*, 2965–2973. https://doi.org/10.1523/JNEUROSCI.4920-10.2011, PubMed: 21414918
Jarvis, M., & Mitra, P. P. (2001). Sampling properties of the spectrum and coherency of sequences of action potentials. *Neural Computation*, *13*, 717–749. https://doi.org/10.1162/089976601300014312, PubMed: 11255566
Kass, R. E., Eden, U. T., & Brown, E. N. (2014). *Analysis of neural data* (Vol. 491). Springer. https://www.stat.cmu.edu/~kass/sam/all/heidiAPR12/all.pdf. https://doi.org/10.1007/978-1-4614-9602-1
Kass, R. E., Ventura, V., & Brown, E. N. (2005). Statistical issues in the analysis of neuronal data. *Journal of Neurophysiology*, *94*, 8–25. https://doi.org/10.1152/jn.00648.2004, PubMed: 15985692

Kotsovolis, G., & Komninos, G. (2009). Awareness during anesthesia: How sure can we be that the patient is sleeping indeed? *Hippokratia*, *13*, 83–89. PubMed: 19561776

Kramer, M. A., & Eden, U. T. (2016). *Case studies in neural data analysis: A guide for the practicing neuroscientist*. MIT Press. https://mark-kramer.github.io/Case-Studies-Python

Krom, A. J., Marmelshtein, A., Gelbard-Sagiv, H., Tankus, A., Hayat, H., Hayat, D., et al. (2020). Anesthesia-induced loss of consciousness disrupts auditory responses beyond primary cortex. *Proceedings of the National Academy of Sciences, U.S.A.*, *117*, 11770–11780. https://doi.org/10.1073/pnas.1917251117, PubMed: 32398367

Lachaux, J.-P., Rodriguez, E., Martinerie, J., & Varela, F. J. (1999). Measuring phase synchrony in brain signals. *Human Brain Mapping*, *8*, 194–208. https://doi.org/10.1002/(SICI)1097-0193(1999)8:4<194::AID-HBM4>3.0.CO;2-C, PubMed: 10619414

Lee, M., Sanders, R. D., Yeom, S.-K., Won, D.-O., Seo, K.-S., Kim, H. J., et al. (2017). Network properties in transitions of consciousness during propofol-induced sedation. *Scientific Reports*, *7*, 16791. https://doi.org/10.1038/s41598-017-15082-5, PubMed: 29196672

Lee, U., Ku, S., Noh, G., Baek, S., Choi, B., & Mashour, G. A. (2013). Disruption of frontal–parietal communication by ketamine, propofol, and sevoflurane. *Anesthesiology*, *118*, 1264–1275. https://doi.org/10.1097/ALN.0b013e31829103f5, PubMed: 23695090

Leslie, K., Sleigh, J., Paech, M. J., Voss, L., Lim, C. W., & Sleigh, C. (2009). Dreaming and electroencephalographic changes during anesthesia maintained with propofol or desflurane. *Anesthesiology*, *111*, 547–555. https://doi.org/10.1097/ALN.0b013e3181adf768, PubMed: 19672164

Lewis, L. D., Ching, S., Weiner, V. S., Peterfreund, R. A., Eskandar, E. N., Cash, S. S., et al. (2013). Local cortical dynamics of burst suppression in the anaesthetized brain. *Brain*, *136*, 2727–2737. https://doi.org/10.1093/brain/awt174, PubMed: 23887187

Lewis, L. D., Voigts, J., Flores, F. J., Schmitt, L. I., Wilson, M. A., Halassa, M. M., et al. (2015). Thalamic reticular nucleus induces fast and local modulation of arousal state. *eLife*, *4*, e08760. https://doi.org/10.7554/eLife.08760, PubMed: 26460547

Lewis, L. D., Weiner, V. S., Mukamel, E. A., Donoghue, J. A., Eskandar, E. N., Madsen, J. R., et al. (2012). Rapid fragmentation of neuronal networks at the onset of propofol-induced unconsciousness. *Proceedings of the National Academy of Sciences, U.S.A.*, *109*, E3377–E3386. https://doi.org/10.1073/pnas.1210907109, PubMed: 23129622

Linderman, S., Antin, B., Zoltowski, D., & Glaser, J. (2020). *SSM: Bayesian learning and inference for state space models*. https://github.com/lindermanlab/ssm

Liu, X., Lauer, K. K., Ward, B. D., Li, S.-J., & Hudetz, A. G. (2013). Differential effects of deep sedation with propofol on the specific and nonspecific thalamocortical systems: A functional magnetic resonance imaging study. *Anesthesiology*, *118*, 59–69. https://doi.org/10.1097/ALN.0b013e318277a801, PubMed: 23221862

Liu, X., Lauer, K. K., Ward, B. D., Rao, S. M., Li, S. J., & Hudetz, A. G. (2012). Propofol disrupts functional interactions between sensory and high-order processing of auditory verbal memory. *Human Brain Mapping*, *33*, 2487–2498. https://doi.org/10.1002/hbm.21385, PubMed: 21932265

Liu, X., Yanagawa, T., Leopold, D. A., Chang, C., Ishida, H., Fujii, N., et al. (2015). Arousal transitions in sleep, wakefulness, and anesthesia are characterized by an orderly sequence of cortical events. *Neuroimage*, *116*, 222–231. https://doi.org/10.1016/j.neuroimage.2015.04.003, PubMed: 25865143

Louis, T. A. (1982). Finding the observed information matrix when using the EM algorithm. *Journal of the Royal Statistical Society: Series B (Methodological)*, *44*, 226–233. https://doi.org/10.1111/j.2517-6161.1982.tb01203.x

Ma, L., Liu, W., & Hudson, A. E. (2019). Propofol anesthesia increases long-range frontoparietal corticocortical interaction in the oculomotor circuit in macaque monkeys. *Anesthesiology*, *130*, 560–571. https://doi.org/10.1097/ALN.0000000000002637, PubMed: 30807382

Miller, K. J., Honey, C. J., Hermes, D., Rao, R. P., Ojemann, J. G., & others. (2014). Broadband changes in the cortical surface potential track activation of functionally diverse neuronal populations. *Neuroimage*, *85*, 711–720. https://doi.org/10.1016/j.neuroimage.2013.08.070, PubMed: 24018305

Mofakham, S., Fry, A., Adachi, J., Stefancin, P. L., Duong, T. Q., Saadon, J. R., et al. (2021). Electrocorticography reveals thalamic control of cortical dynamics following traumatic brain injury. *Communications Biology*, *4*, 1210. https://doi.org/10.1038/s42003-021-02738-2, PubMed: 34675341

Mofakham, S., Liu, Y., Hensley, A., Saadon, J. R., Gammel, T., Cosgrove, M. E., et al. (2022). Injury to thalamocortical projections following traumatic brain injury results in attractor dynamics for cortical networks. *Progress in Neurobiology*, *210*, 102215. https://doi.org/10.1016/j.pneurobio.2022.102215, PubMed: 34995694

Monti, M. M., Lutkenhoff, E. S., Rubinov, M., Boveroux, P., Vanhaudenhuyse, A., Gosseries, O., et al. (2013). Dynamic change of global and local information processing in propofol-induced loss and recovery of consciousness. *PLoS Computational Biology*, *9*, e1003271. https://doi.org/10.1371/journal.pcbi.1003271, PubMed: 24146606

Moody, O. A., Zhang, E. R., Vincent, K. F., Kato, R., Melonakos, E. D., Nehs, C. J., et al. (2021). The neural circuits underlying general anesthesia and sleep. *Anesthesia and Analgesia*, *132*, 1254–1264. https://doi.org/10.1213/ANE.0000000000005361, PubMed: 33857967

Müller, E. J., Munn, B. R., Redinbaugh, M. J., Lizier, J., Breakspear, M., Saalmann, Y. B., et al. (2023). The non-specific matrix thalamus facilitates the cortical information processing modes relevant for conscious awareness. *Cell Reports*, *42*, 112844. https://doi.org/10.1016/j.celrep.2023.112844, PubMed: 37498741

Murphy, K. P. (2023). *Probabilistic machine learning: Advanced topics*. MIT Press. https://probml.github.io/book2

Nghiem, T.-A. E., Tort-Colet, N., Górski, T., Ferrari, U., Moghimyfiroozabad, S., Goldman, J. S., et al. (2020). Cholinergic switch between two types of slow waves in cerebral cortex. *Cerebral Cortex*, *30*, 3451–3466. https://doi.org/10.1093/cercor/bhz320, PubMed: 31989160

Nourski, K. V., Banks, M. I., Steinschneider, M., Rhone, A. E., Kawasaki, H., Mueller, R. N., et al. (2017). Electrocorticographic delineation of human auditory cortical fields based on effects of propofol anesthesia. *Neuroimage*, *152*, 78–93. https://doi.org/10.1016/j.neuroimage.2017.02.061, PubMed: 28254512

Nourski, K. V., Steinschneider, M., Rhone, A. E., Kawasaki, H., Howard, M. A., & Banks, M. I. (2018). Auditory predictive coding across awareness states under anesthesia: An intracranial electrophysiology study. *Journal of Neuroscience*, *38*, 8441–8452. https://doi.org/10.1523/JNEUROSCI.0967-18.2018, PubMed: 30126970

Nourski, K. V., Steinschneider, M., Rhone, A. E., Krause, B. M., Mueller, R. N., Kawasaki, H., et al. (2021). Cortical responses to vowel sequences in awake and anesthetized states: A human intracranial electrophysiology study. *Cerebral Cortex*, *31*, 5435–5448. https://doi.org/10.1093/cercor/bhab168, PubMed: 34117741

Pawitan, Y. (2001). *In all likelihood: Statistical modelling and inference using likelihood*. Oxford University Press.
Pedregosa, F., Varoquaux, G., Gramfort, A., Michel, V., Thirion, B., Grisel, O., et al. (2011). Scikit-learn: Machine learning in Python. *Journal of Machine Learning Research*, *12*, 2825–2830.
Pesaran, B., Vinck, M., Einevoll, G. T., Sirota, A., Fries, P., Siegel, M., et al. (2018). Investigating large-scale brain dynamics using field potential recordings: Analysis and interpretation. *Nature Neuroscience*, *21*, 903–919. https://doi.org/10.1038/s41593-018-0171-8, PubMed: 29942039
Petersen, C. C. H., Hahn, T. T. G., Mehta, M., Grinvald, A., & Sakmann, B. (2003). Interaction of sensory responses with spontaneous depolarization in layer 2/3 barrel cortex. *Proceedings of the National Academy of Sciences, U.S.A.*, *100*, 13638–13643. https://doi.org/10.1073/pnas.2235811100, PubMed: 14595013
Purdon, P. L., Pierce, E. T., Mukamel, E. A., Prerau, M. J., Walsh, J. L., Wong, K. F. K., et al. (2013). Electroencephalogram signatures of loss and recovery of consciousness from propofol. *Proceedings of the National Academy of Sciences, U.S.A.*, *110*, E1142–E1151. https://doi.org/10.1073/pnas.1221180110, PubMed: 23487781
Purdon, P. L., Sampson, A., Pavone, K. J., & Brown, E. N. (2015). Clinical electroencephalography for anesthesiologists: Part I: Background and basic signatures. *Anesthesiology*, *123*, 937–960. https://doi.org/10.1097/ALN.0000000000000841, PubMed: 26275092
Rabiner, L. R. (1989). A tutorial on Hidden Markov Models and selected applications in speech recognition. *Proceedings of the IEEE*, *77*, 257–286. https://doi.org/10.1109/5.18626
Ray, S., & Maunsell, J. H. R. (2011). Different origins of gamma rhythm and high-gamma activity in macaque visual cortex. *PLoS Biology*, *9*, e1000610. https://doi.org/10.1371/journal.pbio.1000610, PubMed: 21532743
Raz, A., Grady, S. M., Krause, B. M., Uhlrich, D. J., Manning, K. A., & Banks, M. I. (2014). Preferential effect of isoflurane on top–down vs. bottom–up pathways in sensory cortex. *Frontiers in Systems Neuroscience*, *8*, 191. https://doi.org/10.3389/fnsys.2014.00191, PubMed: 25339873
Redinbaugh, M. J., Phillips, J. M., Kambi, N. A., Mohanta, S., Andryk, S., Dooley, G. L., et al. (2020). Thalamus modulates consciousness via layer-specific control of cortex. *Neuron*, *106*, 66–75. https://doi.org/10.1016/j.neuron.2020.01.005, PubMed: 32053769
Reig, R., & Sanchez-Vives, M. V. (2007). Synaptic transmission and plasticity in an active cortical network. *PLoS One*, *2*, e670. https://doi.org/10.1371/journal.pone.0000670, PubMed: 17668052
Reig, R., Zerlaut, Y., Vergara, R., Destexhe, A., & Sanchez-Vives, M. V. (2015). Gain modulation of synaptic inputs by network state in auditory cortex in vivo. *Journal of Neuroscience*, *35*, 2689–2702. https://doi.org/10.1523/JNEUROSCI.2004-14.2015, PubMed: 25673859
Rigas, P., & Castro-Alamancos, M. A. (2007). Thalamocortical up states: Differential effects of intrinsic and extrinsic cortical inputs on persistent activity. *Journal of Neuroscience*, *27*, 4261–4272. https://doi.org/10.1523/JNEUROSCI.0003-07.2007, PubMed: 17442810
Sachdev, R. N., Ebner, F. F., & Wilson, C. J. (2004). Effect of subthreshold up and down states on the whisker-evoked response in somatosensory cortex. *Journal of Neurophysiology*, *92*, 3511–3521. https://doi.org/10.1152/jn.00347.2004, PubMed: 15254074
Sahinovic, M. M., Struys, M. M. R. F., & Absalom, A. R. (2018). Clinical pharmacokinetics and pharmacodynamics of propofol. *Clinical Pharmacokinetics*, *57*, 1539–1558. https://doi.org/10.1007/s40262-018-0672-3, PubMed: 30019172
Saxena, N., Muthukumaraswamy, S. D., Diukova, A., Singh, K., Hall, J., & Wise, R. (2013). Enhanced stimulus-induced gamma activity in humans during propofol-induced sedation. *PLoS One*, *8*, e57685. https://doi.org/10.1371/journal.pone.0057685, PubMed: 23483920
Schmitt, L. I., Wimmer, R. D., Nakajima, M., Happ, M., Mofakham, S., & Halassa, M. M. (2017). Thalamic amplification of cortical connectivity sustains attentional control. *Nature*, *545*, 219–223. https://doi.org/10.1038/nature22073, PubMed: 28467827
Seabold, S., & Perktold, J. (2010). Statsmodels: Econometric and statistical modeling with Python. In S. Van der Walt & J. Millman (Eds.), *Proceedings of the 9th Python in Science Conference* (pp. 92–96). https://doi.org/10.25080/Majora-92bf1922-011
Sebel, P. S., Bowdle, T. A., Ghoneim, M. M., Rampil, I. J., Padilla, R. E., Gan, T. J., et al. (2004). The incidence of awareness during anesthesia: A multicenter United States study. *Anesthesia and Analgesia*, *99*, 833–839. https://doi.org/10.1213/01.ANE.0000130261.90896.6C, PubMed: 15333419
Sela, Y., Vyazovskiy, V. V., Cirelli, C., Tononi, G., & Nir, Y. (2016). Responses in rat core auditory cortex are preserved during sleep spindle oscillations. *Sleep*, *39*, 1069–1082. https://doi.org/10.5665/sleep.5758, PubMed: 26856904
Singer, W. (1993). Synchronization of cortical activity and its putative role in information processing and learning. *Annual Review of Physiology*, *55*, 349–374. https://doi.org/10.1146/annurev.ph.55.030193.002025, PubMed: 8466179
Smith, A. C., & Brown, E. N. (2003). Estimating a state-space model from point process observations. *Neural Computation*, *15*, 965–991. https://doi.org/10.1162/089976603765202622, PubMed: 12803953
Song, A. H., Chlon, L., Soulat, H., Tauber, J., Subramanian, S., Ba, D., et al. (2019). Multitaper infinite Hidden Markov Model for EEG. In *41st Annual International Conference of the IEEE Engineering in Medicine and Biology Society (EMBC)* (pp. 5803–5807). IEEE. https://doi.org/10.1109/EMBC.2019.8856817, PubMed: 31947171
Soplata, A. E., Adam, E., Brown, E. N., Purdon, P. L., McCarthy, M. M., & Kopell, N. (2023). Rapid thalamocortical network switching mediated by cortical synchronization underlies propofol-induced EEG signatures: A biophysical model. *Journal of Neurophysiology*, *130*, 86–103. https://doi.org/10.1152/jn.00068.2022, PubMed: 37314079
Steriade, M., McCormick, D. A., & Sejnowski, T. J. (1993). Thalamocortical oscillations in the sleeping and aroused brain. *Science*, *262*, 679–685. https://doi.org/10.1126/science.8235588, PubMed: 8235588
Steriade, M., Timofeev, I., & Grenier, F. (2001). Natural waking and sleep states: A view from inside neocortical neurons. *Journal of Neurophysiology*, *85*, 1969–1985. https://doi.org/10.1152/jn.2001.85.5.1969, PubMed: 11353014
Supp, G. G., Siegel, M., Hipp, J. F., & Engel, A. K. (2011). Cortical hypersynchrony predicts breakdown of sensory processing during loss of consciousness. *Current Biology*, *21*, 1988–1993. https://doi.org/10.1016/j.cub.2011.10.017, PubMed: 22100063
Sweeting, T. J. (1980). Uniform asymptotic normality of the maximum likelihood estimator. *Annals of Statistics*, *8*, 1375–1381. https://doi.org/10.1214/aos/1176345208
Tasserie, J., Uhrig, L., Sitt, J. D., Manasova, D., Dupont, M., Dehaene, S., et al. (2022). Deep brain stimulation of the thalamus restores signatures of consciousness in a nonhuman primate model. *Science Advances*, *8*, eabl5547. https://doi.org/10.1126/sciadv.abl5547, PubMed: 35302854
Tononi, G., Boly, M., Massimini, M., & Koch, C. (2016). Integrated information theory: From consciousness to its physical substrate. *Nature Reviews Neuroscience*, *17*, 450–461. https://doi.org/10.1038/nrn.2016.44, PubMed: 27225071

Torao-Angosto, M., Manasanch, A., Mattia, M., & Sanchez-Vives, M. V. (2021). Up and down states during slow oscillations in slow-wave sleep and different levels of anesthesia. *Frontiers in Systems Neuroscience*, *15*, 609645. https://doi.org/10.3389/fnsys.2021.609645, PubMed: 33633546

Turner, T. R., Cameron, M. A., & Thomson, P. J. (1998). Hidden Markov chains in generalized linear models. *Canadian Journal of Statistics/La Revue Canadienne de Statistique*, *26*, 107–125. https://doi.org/10.2307/3315677

Valli, K., Radek, L., Kallionpää, R. E., Scheinin, A., Långsjö, J., Kaisti, K., et al. (2023). Subjective experiences during dexmedetomidine- or propofol-induced unresponsiveness and non-rapid eye movement sleep in healthy male subjects. *British Journal of Anaesthesia*, *131*, 348–359. https://doi.org/10.1016/j.bja.2023.04.026, PubMed: 37268445

van Kerkoerle, T., Self, M. W., Dagnino, B., Gariel-Mathis, M.-A., Poort, J., van der Togt, C., et al. (2014). Alpha and gamma oscillations characterize feedback and feedforward processing in monkey visual cortex. *Proceedings of the National Academy of Sciences, U.S.A.*, *111*, 14332–14341. https://doi.org/10.1073/pnas.1402773111, PubMed: 25205811

Vijayan, S., Ching, S. N., Purdon, P. L., Brown, E. N., & Kopell, N. J. (2013). Thalamocortical mechanisms for the anteriorization of alpha rhythms during propofol-induced unconsciousness. *Journal of Neuroscience*, *33*, 11070–11075. https://doi.org/10.1523/JNEUROSCI.5670-12.2013, PubMed: 23825412

Virtanen, P., Gommers, R., Oliphant, T. E., Haberland, M., Reddy, T., Cournapeau, D., et al. (2020). SciPy 1.0: Fundamental algorithms for scientific computing in Python. *Nature Methods*, *17*, 261–272. https://doi.org/10.1038/s41592-019-0686-2, PubMed: 32015543

Wegman, E. J., & Wright, I. W. (1983). Splines in statistics. *Journal of the American Statistical Association*, *78*, 351–365. https://doi.org/10.1080/01621459.1983.10477977

Weiner, V. S., Zhou, D. W., Kahali, P., Stephen, E. P., Peterfreund, R. A., Aglio, L. S., et al. (2023). Propofol disrupts alpha dynamics in functionally distinct thalamocortical networks during loss of consciousness. *Proceedings of the National Academy of Sciences, U.S.A.*, *120*, e2207831120. https://doi.org/10.1073/pnas.2207831120, PubMed: 36897972

Zelmann, R., Paulk, A. C., Tian, F., Villegas, G. A. B., Peralta, J. D., Crocker, B., et al. (2023). Differential cortical network engagement during states of un/consciousness in humans. *Neuron*. https://doi.org/10.1016/j.neuron.2023.08.007, PubMed: 37659409